A genetically encoded fluorescent sensor for rapid and specific *in vivo* detection of norepinephrine

Jiesi Feng[1,2,3], Changmei Zhang[4,8], Julieta Lischinsky[5,9,10], Miao Jing[1,2,3], Jingheng Zhou[6], Huan Wang[1,2], Yajun Zhang[1,3,7], Ao Dong[1,2,3], Zhaofa Wu[1,2], Hao Wu[1,2,12], Weiyu Chen[4,8], Peng Zhang[7], Jing Zou[11], S. Andrew Hires[11], J. Julius Zhu[7,13,14,15], Guohong Cui[6], Dayu Lin[5,9,10], Jiulin Du[4,8], Yulong Li[1,2,3,16,*]

[1]State Key Laboratory of Membrane Biology, Peking University School of Life Sciences, Beijing 100871, China

[2]PKU-IDG/McGovern Institute for Brain Research, Beijing 100871, China

[3]Peking-Tsinghua Center for Life Sciences, Academy for Advanced Interdisciplinary Studies, Peking University, Beijing 100871, China

[4]Institute of Neuroscience, State Key Laboratory of Neuroscience, CAS Center for Excellence in Brain Science and Intelligence Technology, Chinese Academy of Sciences, Shanghai 200031, China

[5]Neuroscience Institute, New York University School of Medicine, New York, NY 10016, USA

[6]Neurobiology Laboratory, National Institute of Environmental Health Sciences, National Institutes of Health, Research Triangle Park, NC 27709, USA

[7]Department of Pharmacology, University of Virginia School of Medicine, Charlottesville, VA 22908, USA

[8]University of Chinese Academy of Sciences, Beijing 100049, China

[9]Department of Psychiatry, New York University School of Medicine, New York, NY 10016, USA

[10]Center for Neural Science, New York University, New York, NY 10016, USA

[11]Department of Biological Sciences, Neurobiology Section, University of Southern California, Los Angeles, CA 90089, USA

[12]School of Life Sciences, Tsinghua University, Beijing 100084, China

[13]School of Medicine, Ningbo University, Ningbo, 315010, China

[14]Donders Institute for Brain, Cognition and Behavior, Radboud University Nijmegen, 6525

EN, Nijmegen, Netherlands

[15]Department of Physiology, School of Basic Medicine, Tongji Medical College, Huazhong University of Science and Technology, Wuhan 430030, China

[16]Lead contact

*Manuscript correspondence:

Yulong Li (yulongli@pku.edu.cn)

Acknowledgements

This work was supported by the National Basic Research Program of China (973 Program; grant 2015CB856402), the General Program of National Natural Science Foundation of China (project 31671118), the NIH BRAIN Initiative grant U01NS103558, the Junior Thousand Talents Program of China, the grants from the Peking-Tsinghua Center for Life Sciences, and the State Key Laboratory of Membrane Biology at Peking University School of Life Sciences to Y. L; the Key Research Program of Frontier Sciences (QYZDY-SSW-SMC028) of Chinese Academy of Sciences, and Shanghai Science and Technology Committee (18JC1410100) to J.D.; the NIH grants R01MH101377 and R21HD090563 and an Irma T. Hirschl Career Scientist Award to D.L.; and the Intramural Research Program of the NIH/NIEHS of the United States (1ZIAES103310) to G.C.

We thank Yi Rao for sharing the two-photon microscope and Xiaoguang Lei for the platform support of the Opera Phenix high-content screening system at PKU-CLS. We thank the Core Facilities at the School of Life Sciences, Peking University for technical assistance. We thank Bryan L. Roth and Nevin A. Lambert for sharing stable cell lines and plasmids. We thank Yue Sun, Sunlei Pan, Lun Yang, Haohong Li for inputs on sensors' characterization and application. We thank Yanhua Huang, Liqun Luo and Mickey London for valuable feedback of the manuscript.

Author Contributions

Y. L conceived and supervised the project. J.F., M.J., H.Wang, A.D., and Z.W. performed experiments related to sensor development, optimization, and characterization in culture HEK cells, culture neurons and brain slices. Y.Z., P.Z. and J.J.Z designed and performed experiments using Sindbis virus in slices. C.Z., W.C., and J.D. designed and performed experiments on transgenic fish. J.L., J.Zhou, H.Wu, J.,Zou, S.A.H., G.C., and D.L. designed and performed experiments in behaving mice. All authors contributed to data interpretation and data analysis. Y. L and J.F. wrote the manuscript with input from M.J.,

J.L., and D.L. and help from other authors.

Declaration of Interests

The authors declare competing financial interests. J.F., M.J., H.Wang, and Y. L have filed patent applications whose value might be affected by this publication.

Abstract

Norepinephrine (NE) and epinephrine (Epi), two key biogenic monoamine neurotransmitters, are involved in a wide range of physiological processes. However, their precise dynamics and regulation remain poorly characterized, in part due to limitations of available techniques for measuring these molecules *in vivo*. Here, we developed a family of GPCR Activation-Based NE/Epi ($GRAB_{NE}$) sensors with a 230% peak $\Delta F/F_0$ response to NE, good photostability, nanomolar-to-micromolar sensitivities, sub-second rapid kinetics, high specificity to NE vs. dopamine. Viral- or transgenic- mediated expression of $GRAB_{NE}$ sensors were able to detect electrical-stimulation evoked NE release in the locus coeruleus (LC) of mouse brain slices, looming-evoked NE release in the midbrain of live zebrafish, as well as optogenetically and behaviorally triggered NE release in the LC and hypothalamus of freely moving mice. Thus, $GRAB_{NE}$ sensors are a robust tool for rapid and specific monitoring of *in vivo* NE/Epi transmission in both physiological and pathological processes.

Introduction

Both norepinephrine (NE) and epinephrine (Epi) are key monoamine neurotransmitters in the central nervous systems and peripheral organs of vertebrate organisms. These transmitters play an important role in a plethora of physiological processes, allowing the organism to cope with its ever-changing internal and external environment. In the brain, NE is synthesized primarily in the locus coeruleus (LC), a small yet powerful nucleus located in the pons. Noradrenergic LC neurons project throughout the brain and exert a wide range of effects, including processing sensory information (Berridge and Waterhouse, 2003), regulating the sleep-wake/arousal state (Berridge et al., 2012), and mediating attentional function (Bast et al., 2018). Blocking noradrenergic transmission causes impaired cognition and arousal and is closely correlated with a variety of psychiatric conditions and neurodegenerative diseases, including stress (Chrousos, 2009), anxiety (Goddard et al., 2010), depression (Moret and Briley, 2011), attention-deficit hyperactivity disorder (ADHD) (Berridge and Spencer, 2016), and Parkinson's disease (PD) (Espay et al., 2014). In the sympathetic nervous system, both NE and Epi play a role in regulating heart function (Brodde et al., 2001) and blood pressure (Zimmerman, 1981).

Despite their clear importance in a wide range of physiological processes, the spatial and temporal dynamics of NE and Epi in complex organs (*e.g.* the vertebrate brain) are poorly understood at the *in vivo* level due to limitations associated with current detection methods. Classic detection methods such as microdialysis-coupled biochemical analysis (Bito et al., 1966; Justice, 1993; Watson et al., 2006) have low temporal resolution, requiring a relatively long time (typically 5 min/collection) and complex sampling procedures, thereby limiting the ability to accurately measure the dynamics of noradrenergic activity in the physiological state (Chefer et al., 2009). Recent improvements in microdialysis—in particular, the introduction of the nano-LC-microdialysis method (Lee et al., 2008; Olive et al., 2000)—have significantly increased detection sensitivity; however, this approach is still limited by a relatively slow sampling rate (on the order of several minutes). On the other hand, electrochemical detection techniques based on measuring currents generated by the oxidation of NE/Epi (Bruns, 2004; Park et al., 2009; Robinson et al., 2008; Zhou and Misler, 1995) provide nanomolar sensitivity and millisecond temporal resolution; however, their inability to distinguish NE and Epi from other monoamine neurotransmitters—particularly dopamine (Robinson et al., 2003)—presents a significant physiological limitation with respect to measuring noradrenergic/adrenergic transmission both in *ex vivo* tissue preparations and *in vivo*. In addition, both microdialysis-based and electrochemical techniques are designed to detect volume-averaged NE/Epi levels in the extracellular fluid and therefore cannot provide cell type–specific or subcellular information.

Real-time imaging of NE dynamics would provide an ideal means to non-invasively track NE with high spatiotemporal resolution. A recent innovation in real-time imaging, the cell-based reporters known as CNiFERs (Muller et al., 2014), converts an extracellular NE signal into an intracellular calcium signal that can be measured using highly sensitive

fluorescence imaging. However, CNiFERs require implantation of exogenous cells and can report only volume transmission of NE/Epi. By contrast, genetically encoded sensors, in theory, circumvent the above-mentioned limitations to provide fast, clear, non-invasive, cell type–specific reporting of NE/Epi dynamics. In practice, all genetically encoded NE sensors developed to date have poor signal-to-noise ratio and narrow dynamic range (*e.g.*, a <10% change in FRET ratio under optimal conditions) (Nakanishi et al., 2006; Vilardaga et al., 2003; Wang et al., 2018b), thus limiting their applicability, particularly in *in vivo* applications.

To overcome these limitations, we developed a series of genetically encoded single-wavelength fluorescent $GRAB_{NE}$ sensors with rapid kinetics, a $\Delta F/F_0$ dynamic range of ~200%, and EGFP-comparable spectra, brightness, and photostability. Here, we showcase the wide applicability of our $GRAB_{NE}$ sensors using a number of *in vitro* and *in vivo* preparations. In every application tested, the $GRAB_{NE}$ sensors readily reported robust, chemical-specific NE signals. Thus, our $GRAB_{NE}$ sensors provide a powerful imaging-based probe for measuring the cell-specific regulation of adrenergic/noradrenergic transmission under a wide range of physiological and pathological conditions.

Results

Development and characterization of GRAB$_{NE}$ sensors

Inspired by the structure (Rasmussen et al., 2011a; Rasmussen et al., 2011b) and working mechanism (Chung et al., 2011; Manglik et al., 2015; Nygaard et al., 2013) of the β2 adrenergic G protein–coupled receptor (GPCR), we exploited the conformational change between the fifth and sixth transmembrane domains (TM5 and TM6, respectively) upon ligand binding to modulate the brightness of an attached fluorescent protein. Building upon the successful strategy of generating GPCR activation-based sensors for acetylcholine (GACh) (Jing et al., 2018) and dopamine (GRAB$_{DA}$) (Sun et al., 2018), we first systematically screened human adrenergic receptors as a possible scaffold. We inserted circular permutated EGFP (cpEGFP) into the third intracellular loop domain (ICL3) of three α-adrenergic receptors (α1DR, α2AR, and α2BR) and two β-adrenergic receptors (β2R and β3R) (Fig. 1A). Among these five constructs, we found that α2AR-cpEGFP had the best membrane trafficking, indicated by its high colocalization with membrane-targeted RFP (Fig. S1); we therefore selected this construct as the scaffold for further screening.

The length of the linker surrounding the cpEGFP moiety inserted in G-GECO (Zhao et al., 2011), GCaMP (Akerboom et al., 2012), GACh (Jing et al., 2018), and GRAB$_{DA}$ (Sun et al., 2018) can affect the fluorescence response of cpEGFP-based indicators. Thus, as the next step, we systematically truncated the linker which starts with the entire flexible ICL3 of α2AR surrounding cpEGFP (Fig. 1B). We initially screened 275 linker-length variant proteins and identified a sensor (GRAB$_{NE0.5m}$) with a modest response to NE (Fig. 1B, right). From this scaffold, we performed a random mutation screening of seven amino acids (AAs) in close proximity to the cpEGFP moiety; two of these AAs are on the N-terminal side of cpEGFP, and the remaining five are on the C-terminal side of cpEGFP (Fig. 1C). From approximately 200 mutant versions of GRAB$_{NE0.5m}$, we found that GRAB$_{NE1m}$—which contains a glycine-to-threonine mutation at position C1—provided the best performance with respect to $\Delta F/F_0$ and brightness (Fig. 1C, middle and right).

Next, we expressed GRAB$_{NE1m}$ in HEK293T cells and applied NE in a range of concentrations. NE induced a fluorescence change in GRAB$_{NE1m}$-expressing cells in a dose-dependent manner, with an EC_{50} of 0.93 μM and a maximum $\Delta F/F_0$ of approximately 230% in response to a saturating concentration of NE (100 μM) (Fig. 1D, middle and right). We also introduced mutations in α2AR in order to increase its sensitivity at detecting NE. We found that a single T6.34K point mutation (Ren et al., 1993)—which is close to the highly conserved E6.30 site—resulted in a 10-fold increase in sensitivity (EC_{50} ~83 nM) to NE compared with GRAB$_{NE1m}$; this sensor, which we call GRAB$_{NE1h}$, has a maximum $\Delta F/F_0$ of ~130% in response to 100 μM NE. As a control, we also generated GRAB$_{NEmut}$, which has the mutation S5.46A at the putative ligand-binding pocket and therefore is unable to bind NE (Fig. 1D); this control sensor has similar brightness and membrane trafficking (Fig. S1 and S2A), but does not respond to NE even at 100 μM (Fig. 1D, middle and right).

To examine whether our $GRAB_{NE}$ sensors can capture the rapid dynamic properties of NE signaling, including its release, recycling, and degradation, we bathed $GRAB_{NE1h}$-expressing HEK293T cells in a solution containing NPEC-caged NE; a focused spot of 405-nm light was applied to locally uncage NE by photolysis (Fig. 2A). Transient photolysis induced a robust increase in fluorescence in $GRAB_{NE1h}$-expressing cells (mean on time constant 137ms, single exponential fit), which was blocked by application of the α2-adrenergic receptor antagonist yohimbine (Fig. 2B,C). To characterize both the on and off rates (τ_{on} and τ_{off}, respectively) of the $GRAB_{NE}$ sensors, we locally applied various compounds to $GRAB_{NE}$-expressing cells using rapid perfusion and measured the fluorescence response using high-speed line scanning (Fig. 2D,E). The average delay intrinsic to the perfusion system (measured by fitting the fluorescence increase in the co-applied red fluorescent dye Alexa 568) was 34 ms (Fig. 2F). Fitting the fluorescence change in each sensor with a single exponential function yielded an average τ_{on} of 72 and 36 ms for $GRAB_{NE1m}$ and $GRAB_{NE1h}$, respectively, and an average τ_{off} of 680 and 1890 ms for $GRAB_{NE1m}$ and $GRAB_{NE1h}$, respectively (Fig. 2E,F). The faster on-rate and slower off-rate of $GRAB_{NE1h}$ compared to $GRAB_{NE1m}$ is consistent with its relatively higher affinity for NE.

High ligand specificity is an essential requirement for tools designed to detect structurally similar monoamine-based molecules. Importantly, our $GRAB_{NE}$ sensors, which are based on α2AR, respond to both NE and Epi, but do not respond to other neurotransmitters (Fig. 2G). The sensors also respond to the α2AR agonist brimonidine but not the β2-adrenergic receptor agonist isoprenaline, which indicates receptor-subtype specificity. Moreover, the NE-induced fluorescence increase in $GRAB_{NE}$-expressing cells was blocked by the α-adrenergic receptor antagonist yohimbine, but not the β-adrenergic receptor antagonist ICI 118,551. Additionally, because NE and DA are structurally similar yet functionally distinct, we characterized how our $GRAB_{NE}$ sensors respond to various concentrations of DA and NE. Wild-type α2AR has an 85-fold higher affinity for NE versus DA (Fig. 2H, right); in contrast, $GRAB_{NE1m}$ has a 350-fold higher affinity for NE, whereas $GRAB_{NE1h}$ was similar to the wild-type receptor, with a 37-fold higher affinity for NE (Fig. 2H). In contrast, fast-scan cyclic voltammetry (FSCV) was unable to differentiate between NE and DA, producing a nearly identical response to similar concentrations of NE and DA (Fig. 2I) (Robinson et al., 2003). To test the photostability of our NE sensors, we continuously illuminated $GRAB_{NE}$-expressing HEK293T cells using either 1-photon (confocal) or 2-photon laser microscopy and found that the $GRAB_{NE}$ sensors are more photostable than EGFP under both conditions (Fig. S2C). Taken together, these data suggest that the $GRAB_{NE}$ sensors can be used to measure the dynamic properties of noradrenergic activity with high specificity for NE over other neurotransmitters.

Next, we examined whether our $GRAB_{NE}$ sensors can trigger GPCR-mediated downstream signaling pathways. First, we bathed $GRAB_{NE1m}$-expressing cells in a saturating concentration of NE for 2 h, but found no significant internalization of $GRAB_{NE1m}$ (Fig. 2J).

Similarly, we found that both $GRAB_{NE1m}$ and $GRAB_{NE1h}$ lack β-arrestin–mediated signaling, even at the highest concentration of NE tested (Fig. 2K), suggesting that the $GRAB_{NE}$ sensors are not coupled to β-arrestin signaling. In addition, $GRAB_{NE1m}$ and $GRAB_{NE1h}$ had drastically reduced downstream Gi coupling compared to wild-type α2AR, which was measured using a Gi-coupling–dependent luciferase complementation assay (Fig. 2L) (Wan et al., 2018). We also found that G protein activation by $GRAB_{NE1m}$ measured using the highly sensitive TGFα shedding was reduced by about 100-fold compared to the wild-type receptor (Fig. S2B) (Inoue et al., 2012). Finally, blocking G protein activation by treating cells with pertussis toxin (Fig. 2M) had no effect on the fluorescence response of either $GRAB_{NE1m}$ or $GRAB_{NE1h}$, indicating that the fluorescence response of $GRAB_{NE}$ sensors does not require G protein coupling (Rasmussen et al., 2011a). Taken together, these data indicate that $GRAB_{NE}$ sensors can be used to report NE concentration without inadvertently engaging GPCR downstream signaling.

Characterization of $GRAB_{NE}$ sensors in cultured neurons

The expression, trafficking, and response of proteins can differ considerably between neurons and cell lines (Marvin et al., 2013; Zou et al., 2014). Therefore, to characterize the performance of $GRAB_{NE}$ sensors in neurons, we co-expressed $GRAB_{NE}$ together with several neuronal markers in cultured cortical neurons. Both $GRAB_{NE1m}$ and $GRAB_{NEmut}$ trafficked to the cell membrane and co-localized with the membrane-targeted marker RFP-CAAX (Fig. 3A,B). Upon bath-application of a saturating concentration of NE, $GRAB_{NE1m}$ and $GRAB_{NE1h}$ had a peak $\Delta F/F_0$ of approximately 230% and 150%, respectively, whereas $GRAB_{NEmut}$ had no response (Fig. 3D,E); these results are similar to our results obtained with HEK293T cells. Moreover, the NE-induced response in $GRAB_{NE1m}$-expressing cells was similar among various subcellular compartments identified by co-expressing $GRAB_{NE1m}$ with either the axonal marker synaptophysin (SYP) or the dendritic marker PSD95 suggesting that $GRAB_{NE}$ sensors enable the detection of NE throughout the neurons (Fig. 3C). Both $GRAB_{NE1m}$- and $GRAB_{NE1h}$-expressing neurons had a dose-dependent fluorescence increase in response to NE, with mean EC_{50} values of 1.9 μM and 93 nM, respectively (Fig. 3F). Consistent with high selectivity for NE, $GRAB_{NE1m}$ and $GRAB_{NE1h}$ have a 1000-fold and 7-fold higher affinity, respectively, for NE versus DA (Fig. 3F). Moreover, $GRAB_{NE1m}$ responded specifically to NE and Epi, but did not respond to several other neurotransmitters and ligands, including the β2-adrenergic receptor agonist isoprenaline, histamine, dopamine, and serotonin (Fig. 3G). Finally, culturing $GRAB_{NE1m}$-expressing neurons in 100 μM NE for one hour did not cause internalization of the sensor, and the fluorescence increase was both stable for the entire hour and blocked completely by the α2-adrenergic receptor antagonist yohimbine (Fig. 3H,I). Thus, our $GRAB_{NE}$ sensors have the necessary affinity and specificity to faithfully measure noradrenergic signaling in neurons.

Characterization of $GRAB_{NE}$ sensors in both cultured and acute brain slices

To further test the $GRAB_{NE}$ sensors *in vitro*, we expressed $GRAB_{NE1m}$ and $GRAB_{NE1h}$ in cultured hippocampal slices using a Sindbis virus expression system (Fig. S3A). In both $GRAB_{NE1m}$-expressing CA1 neurons and $GRAB_{NE1h}$-expressing CA1 neurons, exogenous application of NE in ACSF—but not ACSF alone—evoked a robust increase in fluorescence (Fig. S3B-D). In contrast, NE had no detectable effect on $GRAB_{NEmut}$-expressing neurons (Fig. S3C,D). Application of several α-adrenergic receptor agonists, including epinephrine and brimonidine, also generated a fluorescence increase in $GRAB_{NE1m}$-expressing neurons (Fig. S3C,F), consistent with data obtained using cultured cells. The rise and decay kinetics of the change in fluorescence were second-order, which reflects the integration of the time required to puff the drugs onto the cells and the sensor's response kinetics (Fig. S3E,G). We also prepared acute hippocampal slices in which $GRAB_{NE1h}$ was expressed using an adeno-associated virus (AAV); in this acute slice preparation, the $GRAB_{NE1h}$-expressing hippocampal neurons are innervated by noradrenergic fibers, which was confirmed by post-hoc staining using an antibody against dopamine beta hydroxylase (Fig. S3H,I). Application of electrical stimuli at 20 Hz for 1 s elicited a robust increase in $GRAB_{NE1h}$ fluorescence, and this increase was blocked by the application of yohimbine (Fig. S3J). Consistent with our results obtained using cultured slices, exogenous application of various α-adrenergic receptor agonists, including NE, Epi, and brimonidine—but not the β-adrenergic receptor agonist isoprenaline—evoked a fluorescence increase in $GRAB_{NE1h}$-expressing neurons, and this response was blocked by yohimbine, but not by the β-adrenergic receptor antagonist ICI 118,551 (Fig. S3K).

Next, we examined whether our $GRAB_{NE}$ sensors can be used to monitor the dynamics of endogenous NE. We expressed $GRAB_{NE1m}$ in the locus coeruleus (LC), which contains the majority of adrenergic neurons within the brain (Fig. 4A). Two weeks after AAV injection, we prepared acute brain slices and observed $GRAB_{NE1m}$ expression in the membrane of LC neurons using two-photon microscopy (Fig. 4A). We then used electrical stimuli to evoke the release of endogenous NE in the LC in the acute slices. Applying one or two stimuli did not produce a detectable fluorescence increase in $GRAB_{NE1m}$-expressing neurons; in contrast, applying 10 or more stimuli at 20 Hz caused a progressively stronger response (Fig. 4B). Application of the voltage-activated potassium channel blocker 4-aminopyridine, which increases Ca^{2+} influx during the action potential, significantly increased the fluorescence response, whereas application of Cd^{2+} to block calcium channels abolished the stimulation-induced fluorescence increase (Fig. 4C), consistent with presynaptic NE release being mediated by Ca^{2+} influx. We also performed line-scanning experiments in order to track the kinetics of NE release (Fig. 4D, left). A brief electrical stimulation induced a rapid fluorescence response with a mean τ_{on} and τ_{off} of 37 ms and 600 ms, respectively (Fig. 4D, middle and right). Taken together, these data indicate that $GRAB_{NE1m}$ can be used to monitor the release of endogenous NE in real time.

NE released into the synapse is recycled back into the presynaptic terminal by the norepinephrine transporter (NET). We therefore tested the sensitivity of $GRAB_{NE1m}$ to NET blockade using desipramine. In the presence of desipramine, electrical stimuli caused a larger fluorescence response in $GRAB_{NE1m}$-expressing neurons compared to ACSF alone (Fig. 4E). Moreover, desipramine significantly slowed the τ_{off} of the fluorescence signal, consistent with reduced reuptake of extracellular NE into the presynaptic terminal. To rule out the possibility that the change in the fluorescence response was caused by a change in synaptic modulation over time, we applied repetitive electrical stimuli at 5-min intervals to $GRAB_{NE1m}$-expressing neurons and found that the stimulation-evoked response was stable for up to 40 min (Fig. 4F). Finally, we examined the specificity of the stimulation-induced response. Compared with a robust response in control conditions, the α-adrenergic antagonist yohimbine blocked the response; moreover, no response was elicited in LC neurons expressing $GRAB_{NEmut}$ or in LC neurons expressing a dopamine version of the sensor ($GRAB_{DA1m}$) (Fig. 4G). In contrast, cells expressing $GRAB_{DA1m}$ responded robustly to the application of DA, and the $GRAB_{NE1m}$ and $GRAB_{DA1m}$ responses were abolished by yohimbine and the dopamine receptor antagonist haloperidol, respectively (Fig. 4H). Taken together, these data indicate that $GRAB_{NE1m}$ is both sensitive and specific for detecting endogenous noradrenergic activity in LC neurons.

$GRAB_{NE1m}$ detects both exogenous NE application and endogenous NE release in awake zebrafish

Zebrafish is both a genetically accessible vertebrate species and an optically transparent organism, thus serving as a suitable model for *in vivo* imaging. We generated the transgenic zebrafish line Tg(HuC:NE1m), which pan-neuronally expresses the $GRAB_{NE1m}$ sensor. Pan-neuronal expression was confirmed by $GRAB_{NE1m}$ fluorescence on the cell membrane of neurons throughout the brain (Fig. 5A). Bath application of 50 μM NE—but not DA at the same concentration—elicited a robust increase in fluorescence intensity that was blocked completely by the subsequent application of 50 μM yohimbine (Fig. 5B-D). In addition, a separate zebrafish line expressing $GRAB_{NEmut}$ did not respond to NE (Fig. 5C,D). Taken together, these data indicate that $GRAB_{NE1m}$ can be used to measure NE in an *in vivo* model.

Next, we investigated whether $GRAB_{NE1m}$ can be used to measure the dynamics of endogenous noradrenergic activity induced by a visual looming stimulus, which triggers a robust escape response in zebrafish. We applied repetitive looming stimuli while using confocal imaging to measure the fluorescence of $GRAB_{NE1m}$-expressing neurites in the optic tectum (Fig. 5E). Each looming stimulus induced a time-locked increase in $GRAB_{NE1m}$ fluorescence, which was blocked by bath application of yohimbine but was unaffected by the β-adrenergic receptor antagonist ICI 118,551 (Fig. 5F,G). In contrast, the same looming stimuli had no effect in animals expressing $GRAB_{NEmut}$ (Fig. 5F,G). In addition, adding

desipramine to block NE reuptake slowed the decay of the fluorescence signal (Fig. 5H). By sparse expression of $GRAB_{NE1m}$ in individual neurons in zebrafish larvae via transient transfection, we were also able to record robust signals corresponding to NE release at single-cell resolution in response to repetitive looming stimuli (Fig. 5I-K), confirming that our $GRAB_{NE}$ sensors can be used to sense NE release at a single-cell level with high spatiotemporal resolution.

$GRAB_{NE1m}$ detects optogenetically evoked NE release in freely moving mice

Having demonstrated the proof-of-concept in a relatively simple *in vivo* vertebrate system, we next examined whether the $GRAB_{NE}$ sensors can be used to monitor the noradrenergic activity in the mammalian brain by virally expressing $GRAB_{NE1m}$ (non-Cre dependent) together with the optogenetic actuator C1V1 (Cre-dependent) in the LC of Th-Cre mice (Fig. 6A). Optogenetic stimulation of LC NE neurons using 561 nm laser pulses reliably evoked an increase in $GRAB_{NE1m}$ fluorescence in fiber photometry recording of freely moving mice. Moreover, Intraperitoneal (i.p.) injection of desipramine produced a slow progressive increase in basal $GRAB_{NE1m}$ fluorescence (consistent with an increase in extracellular NE levels) and caused an increase in the magnitude and decay time of the light-activated responses. I.p. injection of yohimbine abolished both the increase in basal $GRAB_{NE1m}$ fluorescence and the light-evoked responses (Fig. 6B-D). In contrast, treating mice with either GBR 12909 (a selective blocker of dopamine transporters) or eticlopiride (a specific D2R antagonist) had no effect on the light-evoked responses in $GRAB_{NE1m}$ fluorescence (Fig. 6C-E). To further test the selectivity of $GRAB_{NE1m}$ between NE and dopamine, we co-expressed $GRAB_{NE1m}$ and DIO-C1V1 both in the LC and in the substantia nigra pars compacta (SNc) of Th-Cre mice (Fig. 6F). In these mice, optogenetic stimulation of dopamine neurons in the SNc did not cause any changes in the $GRAB_{NE1m}$ fluorescence in the SNc. In contrast, stimulating NE neurons in the LC produced a clear increase in $GRAB_{NE1m}$ fluorescence (Fig. 6F, G). These results confirm that the increase of $GRAB_{NE1m}$ fluorescence reflects the release of endogenous NE from noradrenergic neurons in the LC.

Using $GRAB_{NE1m}$ to track endogenous NE dynamics in the mouse hypothalamus during freely moving behaviors

In the brain, the hypothalamus mediates a variety of innate behaviors essential for survival, including feeding, aggression, mating, parenting, and defense (Hashikawa et al., 2016; Sokolowski and Corbin, 2012; Yang and Shah, 2016). The hypothalamus receives extensive noradrenergic projections (Moore and Bloom, 1979; Schwarz and Luo, 2015; Schwarz et al., 2015) and expresses an abundance of α2-adrenergic receptors (Leibowitz, 1970; Leibowitz et al., 1982). Microdialysis studies found that the hypothalamus is among the brain regions that contains high level of NE during stress (McQuade and Stanford,

2000; Pacak et al., 1995; Shekhar et al., 2002; Tanaka, 1999). To better understand the dynamics of NE signaling in the hypothalamus under stress, we virally expressed hSyn-$GRAB_{NE1m}$ in the lateral hypothalamus of C57BL/6 mice. Three weeks after virus injection, we performed fiber photometry recordings of $GRAB_{NE1m}$ fluorescence during a variety of stressful and non-stressful behaviors in freely moving mice (Fig. 7).

During forced swim test and tail suspension test (both of which were stressful), we observed a significant increase in $GRAB_{NE1m}$ fluorescence. During forced swim test, the fluorescence signal increased continuously regardless of the animal's movements and started to decrease only after the animal was removed from the water (Fig. 7C1-E1). During the 60-s tail suspension test, the signal began to rise when the animal was first pursued by the experimenter's hand, increased continuously while the animal was suspended by the tail, and decreased rapidly back to baseline levels when the animal was returned to its home cage (Fig. 7C2-E2). Additionally, when a human hand was placed in front of the animal, we observed a small and transient increase in $GRAB_{NE1m}$ fluorescence (Fig. 7C3-E3). In contrast, the presence of a non-aggressive mouse of either the same or the opposite sex or close social interaction with the conspecific (7C4-E4, C5-E5) caused no significant change in $GRAB_{NE1m}$ fluorescence. Lastly, neither sniffing nor eating a food attractant—in this case, peanut butter—had an effect on $GRAB_{NE1m}$ fluorescence (Fig. 7C6-E6). These data provide evidence that noradrenergic activity in the lateral hypothalamus occurs primarily under stressful conditions.

Finally, to confirm that the $GRAB_{NE1m}$ sensor indeed detects changes in NE concentration instead of other monoamine neurotransmitters, such as dopamine, we injected mice with a specific NET inhibitor atomoxetine (3 mg/kg i.p.) to inhibit the reuptake of NE. Although atomoxetine had no effect on the peak change in $GRAB_{NE1m}$ fluorescence during the tail suspension test, it significantly slowed the return to baseline levels after each tail suspension (Fig. 7F1-I1); in contrast, treating mice with the α-adrenergic receptor antagonist yohimbine (2 mg/kg) both decreased the peak change in $GRAB_{NE1m}$ fluorescence and significantly accelerated the return to baseline (Fig. 7F1-I1). Treating mice with either the selective DAT inhibitor GBR 12909 (10 mg/kg, i.p.) or the D2 receptor antagonist sulpiride (50 mg/kg, i.p.) had no effect on the peak change in $GRAB_{NE1m}$ fluorescence or the time to return to baseline (Fig. 7F2-I2). In summary, these data demonstrate that our $GRAB_{NE}$ sensors are suitable for monitoring endogenous noradrenergic activity in real time, with high spatiotemporal precision, during freely moving behavior in mammals.

Discussion

Here, we report the development and validation of $GRAB_{NE1m}$ and $GRAB_{NE1h}$, two genetically encoded norepinephrine/epinephrine sensors that can be used both *in vitro* and *in vivo* to monitor noradrenergic activity with high temporal and spatial resolution, high ligand specificity, and cell type specificity. In mouse acute brain slices, our $GRAB_{NE}$ sensors detected NE release from the LC in response to electrical stimulation. In zebrafish, the $GRAB_{NE}$ sensors reported looming-induced NE release with single-cell resolution. In mice, the $GRAB_{NE}$ sensors reported the time-locked release of NE in the LC triggered by optogenetic stimulation, as well as changes in hypothalamic NE levels during a variety of stress-related behaviors.

Compared to existing methods for detecting NE, our $GRAB_{NE}$ sensors have several distinct advantages. First, NE has been difficult to distinguish from DA *in vivo* (*e.g.* by fast-scan cyclic voltammetry) (Park et al., 2009; Robinson et al., 2003), largely because of their structural similarities with only one hydroxyl group difference. Our $GRAB_{NE}$ sensors have extremely high *specificity* for NE over other neurotransmitters and chemical modulators, including DA (Figs. 2H, 3F). $GRAB_{NE1m}$ has a roughly 1000-fold higher affinity for NE over DA when expressed in neurons, even better than the 85-fold difference of the wild-type α2-adrenergic receptor. Thus, our $GRAB_{NE}$ sensors provide new opportunities to probe the dynamics of noradrenergic activity with high specificity, which is particularly valuable when studying the many brain regions that receive overlapping dopaminergic and noradrenergic inputs. One thing to note is that $GRAB_{NE}$ sensors are engineered from the α2a receptor, which may not be suitable for pharmacological investigation of α2a receptor related regulations.

Second, our $GRAB_{NE}$ sensors have extremely high *sensitivity* for NE. Specifically, the EC_{50} for NE approaches sub-micromolar levels, with a 200%—or higher—increase in fluorescence intensity upon binding NE. By comparison, recently published FRET-based NE indicators produce a signal change of ≤10% under optimal conditions (Wang et al., 2018a; Wang et al., 2018b). Thus, $GRAB_{NE}$ sensors have much improved characteristics to monitor endogenous *in vivo* NE dynamics. Third, $GRAB_{NE}$ sensors have brightness and photostability properties that rival EGFP, which permits stable recordings across extended experimental sessions. Fourth, because they provide sub-second response kinetics and are genetically encoded, our $GRAB_{NE}$ sensors can non-invasively report noradrenergic activity *in vivo* with single-cell resolution and a high recording rate (~30 Hz). Finally, because the $GRAB_{NE}$ sensors can traffic to various surface membranes, including the cell body, dendrites, and axons, and because they perform equally well in these membrane compartments, they can provide subcellular spatial resolution, which is essential for understanding compartmental NE signaling *in vivo*.

Ligand binding to endogenous GPCRs drives G-protein activation and receptor internalization. If present in $GRAB_{NE}$ sensors, these responses could interfere with

endogenous signaling fidelity and disrupt normal neuronal activity. To assess this risk, we characterized the downstream coupling of our $GRAB_{NE}$ sensors with both G protein–independent and G protein–dependent pathways. Importantly, the introduction of the cpEGFP moiety in the $GRAB_{NE}$ sensors resulted in non-detectable engagement of arrestin-mediated desensitization/internalization, which ensures more consistent surface expression of the sensor and that the $GRAB_{NE}$ sensors do not inadvertently activate arrestin-dependent signaling. With respect to G protein–dependent signaling, we found that although physiological levels of NE robustly induce a change in $GRAB_{NE1m}$ fluorescence, they do not engage downstream G protein signaling (Fig. 2J-M).

Noradrenergic projections throughout the brain originate almost exclusively from the LC, and NE release plays a role in a wide range of behaviors, including cognition and the regulation of arousal, attention, and alertness (Berridge and Waterhouse, 2003; Li et al., 2018; Schwarz et al., 2015). In this respect, it is interesting to note that our *in vivo* experiments revealed that $GRAB_{NE}$ sensors can reliably report looming-evoked NE release in the optic tectum of live zebrafish. Moreover, our fiber photometry recordings of $GRAB_{NE}$ sensors in the hypothalamus of freely behaving mice revealed specific changes in noradrenergic activity under stressful conditions (e.g., a tail lift or forced swimming), whereas non-stressful conditions such as feeding and social interaction did not appear to alter noradrenergic activity. These data are generally consistent with previous data obtained using microdialysis to measure NE (McQuade and Stanford, 2000; Pacak et al., 1995; Shekhar et al., 2002; Tanaka, 1999). Importantly, however, our approach yielded a more temporally precise measurement of noradrenergic activity with the promise of higher spatial and cell-type specificity.

NE circuits of the LC receive heterogeneous inputs from a broad range of brain regions and send heterogeneous outputs to many brain regions (Schwarz et al., 2015). Congruously, altered noradrenergic activity has been associated with a broad range of brain disorders and conditions, including ADHD, PD, depression, and anxiety (Marien et al., 2004). The complexity of these disorders may, in part, reflect the complexities of noradrenergic circuits and signals, which previous tools have been unable to fully dissect. Thus, understanding the regulation and impact of noradrenergic activity during complex behavior demands technological advances, such as the $GRAB_{NE}$ sensors we present here. Deploying these in concert with other cell-specific tools for reporting (Jing et al., 2018; Patriarchi et al., 2018; Sun et al., 2018) and manipulating neurotransmitter levels (Fenno et al., 2011; Urban and Roth, 2015) should increase our understanding of the circuits and mechanisms that underlie brain functions in both health and diseases.

Experimental model and subject details

Primary cultures

Rat cortical neurons were prepared from postnatal day 0 (P0) Sprague-Dawley rat pups (both male and female, randomly selected; Beijing Vital River). In brief, cortical neurons were dissociated from dissected P0 rat brains in 0.25% Trypsin-EDTA (Gibco), plated on 12-mm glass coverslips coated with poly-D-lysine (Sigma-Aldrich), and cultured at 37°C in 5% CO_2 in neurobasal medium (Gibco) containing 2% B-27 supplement, 1% GlutaMax, and 1% penicillin-streptomycin (Gibco).

Cell lines

HEK293T cells were obtained from ATCC (CRL-3216) and verified based on their morphology under the microscope and by their growth curve. Stable cell lines expressing the wild-type α2-adrenergic receptor or various $GRAB_{NE}$ sensors were constructed by co-transfecting cells with the pPiggyBac plasmid carrying target genes with Tn5 transposase into a stable HEK293T-based cell line expressing chimeric Gαq/i and AP-TGFα (Inoue et al., 2012). Cells that stably expressed the target genes were selected by treating with 2 mg/ml Puromycin (Sigma) after reaching 100% confluence. The HTLA cells used for the TANGO Assay stably express a tTA-dependent luciferase reporter and a β-arrestin2-TEV fusion gene and were a gift from Bryan L. Roth (Kroeze et al., 2015). All cell lines were cultured at 37°C in 5% CO_2 in DMEM (Gibco) supplemented with 10% (v/v) fetal bovine serum (Gibco) and 1% penicillin-streptomycin (Gibco).

Mice

All procedures regarding animals were approved by the respective Animal Care and Use Committees at Peking University, New York University, University of Southern California and the US National Institutes of Health, and were performed in compliance with the US National Institutes of Health guidelines for the care and use of laboratory animals. Wild-type Sprague-Dawley rat pups (P0) were used to prepare cultured cortical neurons. Wild-type C57BL/6 and Th-Cre mice (MMRRC_031029-UCD, obtained from MMRRC) were used to prepare the acute brain slices and for the *in vivo* mouse experiments. Experimental Th-Cre mice were produced by breeding Th-Cre hemizygous BAC transgenic mice with C57BL/6J mice. All animals were housed in the animal facility and were family-housed or pair-housed in a temperature-controlled room with a 12hr-12h light-dark cycle (10 pm to 10 am light) with food and water provided *ad libidum*. All *in vivo* mouse experiments were performed using 2-12-month-old mice of both sexes.

Zebrafish

The background strain for these experiments is the albino strain slc45a2b4. To generate transgenic zebrafish, Both the pTol2-HuC:$GRAB_{NE1m}$ plasmid and Tol2 mRNA were co-injected into single-cell stage zebrafish eggs, and the founders of HuC:NE1m were

screened. HuC:NEmut transgenic fish were generated as described above using the pTol2-HuC:GRAB$_{NEmut}$ plasmid. Adult fish and larvae were maintained on a 14h-10h light-dark cycle at 28°C. All experimental larvae were raised to 6-8 days post-fertilization (dpf) in 10% Hank's solution, which consisted of (in mM): 140 NaCl, 5.4 KCl, 0.25 Na_2HPO_4, 0.44 KH_2PO_4, 1.3 $CaCl_2$, 1.0 $MgSO_4$, and 4.2 $NaHCO_3$ (pH 7.2). Larval zebrafish do not undergo sex differentiation prior to 1 month post-fertilization (Singleman and Holtzman, 2014).

Method details

Molecular cloning

The molecular clones used in this study were generated by Gibson Assembly using DNA fragments amplified using primers (Thermo Fisher Scientific) with 25-bp overlap. The Gibson Assembly cloning enzymes consisted of T5-exonuclease (New England Biolabs), Phusion DNA polymerase (Thermo Fisher Scientific), and Taq ligase (iCloning). Sanger sequencing was performed using the sequencing platform at the School of Life Sciences of Peking University in order to verify the sequence of all clones. All cDNAs encoding the candidate GRAB$_{NE}$ sensors were cloned into the pDisplay vector (Invitrogen) with an upstream IgK leader sequence and a downstream IRES-mCherry-CAAX cassette to label the cell membrane. The cDNAs of select adrenergic receptor candidates were amplified from the human GPCR cDNA library (hORFeome database 8.1), and cpEGFP from GCaMP6s was inserted into the third intracellular loop (ICL3). The insertion sites for the GRAB$_{NE}$ sensors were screened by truncating the ICL3 of the α2-adrenergic receptor at the 10-amino acid (AA) level, followed by fine-tuning at the 1-AA level. Coupling linkers were randomized by PCR amplification using randomized NNB codons in target sites. Other cDNAs used to express the GRAB$_{NE}$ sensors in neurons were cloned into the pAAV vector using the human synapsin promoter (hSyn) or TRE promoter. pAAV-CAG-tTA was used to drive expression of the TRE promoter. The plasmids carrying compartmental markers were cloned by fusing EGFP-CAAX, RFP-CAAX (mScarlet), KDELR-EGFP, PSD95-RFP, and synaptophysin-RFP into the pDest vector. To characterize signaling downstream of the GRAB$_{NE}$ sensors, we cloned the sensors and the wild-type α2-adrenergic receptor into the pTango and pPiggyBac vector, respectively. GRAB$_{NE1m}$-SmBit and α2AR-SmBit constructs were derived from β2AR-SmBit (Wan et al., 2018) using a BamHI site incorporated upstream of the GGSG linker. LgBit-mGsi was a gift from Nevin A. Lambert.

Expression of GRAB$_{NE}$ sensors in cultured cells and in vivo

The GRAB$_{NE}$ sensors were characterized in HEK293T cells and cultured rat cortical neurons, with the exception of the TANGO assay and TGFα shedding assay. HEK293T cells were passaged with Trypsin-EDTA (0.25%, phenol red; Gibco) and plated on 12-mm

size 0 glass coverslips in 24-well plates and grown to ~70% confluence for transfection. HEK293T cells were transfected by incubating cells with a mixture containing 1 μg of DNA and 3 μg of PEI for 6 h. Imaging was performed 24-48 h after transfection. Cells expressing $GRAB_{NE}$ sensors for screening were plated on 96-well plates (PerkinElmer).

Cultured neurons were transfected using the calcium phosphate method at 7-9 DIV. In brief, the neurons were incubated for 2 h in a mixture containing 125 mM $CaCl_2$, HBS (pH 7.04), and 1.5 μg DNAh. The DNA-$Ca_3(PO4)_2$ precipitate was then removed from the cells by washing twice with warm HBS (pH 6.80). Cells were imaged 48 h after transfection.

For *in vivo* expression, the mice were anesthetized by an i.p. injection of 2,2,2-tribromoethanol (Avetin, 500 mg/kg body weight, Sigma-Aldrich), and then placed in a stereotaxic frame for injection of AAVs using a Nanoliter 2000 Injector (WPI) or Nanoject II (Drummond Scientific) microsyringe pump. For the experiments shown in Figures 4 and 6, the AAVs containing hSyn-$GRAB_{NE1m/NE1mut/DA1m}$ and Ef1a-DIO-C1V1-YFP were injected into the LC (AP: -5.45 mm relative to Bregma; ML: ±1.25 mm relative to Bregma; and DV: -2.25 mm from the brain surface) or SNc (AP: -3.1 mm relative to Bregma; ML: ±1.5 mm relative to Bregma; and DV: -3.8 mm from the brain surface) of wild-type or Th-Cre mice. For the experiments shown in Figure 7, 100 nl of AAV9-hSyn-$GRAB_{NE1m}$ (Vigene, $1x10^{13}$ titer genomic copies per ml) were unilaterally into the hypothalamus (AP: -1.7 mm relative to Bregma; ML: 0.90 mm relative to Bregma; and DV: -6.05 mm from the brain surface) of wild-type (C57BL/6) mice at a rate of 10 nl/min.

Fluorescence imaging of HEK293T cells and cultured neurons

HEK293T cells and cultured neurons expressing $GRAB_{NE}$ sensors were screened using an Opera Phenix high-content imaging system (PerkinElmer) and imaged using an inverted Ti-E A1 confocal microscope (Nikon). A 60x/1.15 NA water-immersion objective was mounted on the Opera Phenix and used to screen $GRAB_{NE}$ sensors with a 488-nm laser and a 561-nm laser. A 525/50 nm and a 600/30 nm emission filter were used to collect the GFP and RFP signals, respectively. HEK293T cells expressing $GRAB_{NE}$ sensors were first bathed in Tyrode's solution and imaged before and after addition of the indicated drugs at the indicated concentrations. The change in fluorescence intensity of the $GRAB_{NE}$ sensors was calculated using the change in the GFP/RFP ratio. For confocal microscopy, the microscope was equipped with a 40x/1.35 NA oil-immersion objective, a 488-nm laser, and a 561-nm laser. A 525/50 nm and a 595/50 nm emission filter were used to collect the GFP and RFP signals, respectively. $GRAB_{NE}$-expressing HEK293T cells and neurons were perfused with Tyrode's solutions containing the drug of interest in the imaging chamber. The photostability of $GRAB_{NE}$ sensors and EGFP was measured using a confocal microscope (for 1-photon illumination) equipped with a 488-nm laser at a power setting of ~350 μW, and using a FV1000MPE 2-photon microscope (Olympus, 2-photon illumination) equipped with a 920-nm laser at a power setting of ~27.5 mW. The illuminated region was the entire HEK293T cell expressing the target protein, with an area of ~200 μm^2. Photolysis

of NPEC-caged-NE (Tocris) was performed by combining fast scanning with a 76-ms pulse of 405-nm laser illumination by a confocal microscope.

TANGO assay

NE at various concentrations (ranging from 0.1 nM to 100 μM) was applied to α2AR-expressing or NE1m-/NE1h-expressing HTLA cells (Kroeze et al., 2015). The cells were then cultured for 12 hours to allow expression of the luciferase gene. Furimazine (NanoLuc Luciferase Assay, Promega) was then applied to a final concentration of 5 μM, and luminescence was measured using a VICTOR X5 multilabel plate reader (PerkinElmer).

TGFα shedding assay

Stable cell lines expressing Gαi-AP-TGFα together with the wild-type α2AR or $GRAB_{NE}$ sensors were plated in a 96-well plate and treated by the addition of 10 μl of a 10x solution of NE in each well, yielding a final NE concentration ranging from 0.1 nM to 100 μM. Absorbance at 405 nm was read using a VICTOR X5 multilabel plate reader (PerkinElmer). TGFα release was calculated as described previously (Inoue et al., 2012). Relative levels of G protein activation were calculated as the TGFα release of $GRAB_{NE}$ sensors normalized to the release mediated by wild-type α2AR.

FSCV

Fast-scan cyclic voltammetry was performed using 7-μm carbon fiber microelectrodes. Voltammograms were measured with a triangular potential waveform from −0.4 V to +1.1 V at a scan rate of 400 V/s and a 100-ms interval. The carbon fiber microelectrode was held at −0.4 V between scans. Voltammograms measured in the presence of various different drugs in Tyrode's solution were generated using the average of 200 scans followed by the subtraction of the average of 200 background scans. Currents were recorded using the Pinnacle tethered FSCV system (Pinnacle Technology). Pseudocolor plots were generated using Pinnacle FSCV software. The data were processed using Excel (Microsoft) and plotted using Origin Pro (OriginLab).

Luciferase complementation assay

The luciferase complementation assay was performed as previously described (Wan et al., 2018). In brief, ~48h after transfection the cells were washed with PBS, harvested by trituration, and transferred to opaque 96-well plates containing diluted NE solutions. Furimazine (Nano-Glo; 1:1000; Promega) was added to each well immediately prior to performing the measurements with Nluc.

Fluorescence imaging of $GRAB_{NE}$ in brain slices

Fluorescence imaging of acute brain slices was performed as previously described (Sun et al., 2018). In brief, the animals were anesthetized with Avertin, and acute brain slices containing the LC region or the hippocampus region were prepared in cold slicing buffer

containing (in mM): 110 choline-Cl, 2.5 KCl, 1.25 NaH_2PO_4, 25 $NaHCO_3$, 7 $MgCl_2$, 25 glucose, and 2 $CaCl_2$. Slices were allowed to recover at 35°C in oxygenated Ringers solution containing (in mM): 125 NaCl, 2.5 KCl, 1.25 NaH_2PO_4, 25 $NaHCO_3$, 1.3 $MgCl_2$, 25 glucose, and 2 $CaCl_2$ for at least 40 minutes before experiments. An Olympus FV1000MPE two-photon microscope equipped with a 40x/0.80 NA water-immersion objective and a mode-locked Mai Tai Ti:Sapphire laser (Spectra-Physics) tuned to 920 nm were used for imaging the slices. For electrical stimulation, a concentric electrode (model #CBAEC75, FHC) was positioned near the LC region, and the imaging and stimuli were synchronized using an Arduino board controlled using a custom-written program. The imaging speed was set at 0.148 s/frame with 128 x 96 pixels in each frame. The stimulation voltage was set at ~6 V, and the duration of each stimulation was typically 1 ms. Drugs were either delivered via the perfusion system or directly bath-applied in the imaging chamber.

For immunostaining of brain sections, $GRAB_{NE}$-expressing mice were anesthetized with Avetin, and the heart was perfused with 0.9% NaCl followed by 4% paraformaldehyde (PFA). The brain was then removed, placed in 4% PFA for 4 h, and then cryoprotected in 30% (w/v) sucrose for 24 h. The brain was embedded in tissue-freezing medium, and 50-μm thick coronal sections were cut using a Leica CM1900 cryostat (Leica, Germany). A chicken anti-GFP antibody (1:500, Abcam, #ab13970) was used to label $GRAB_{NE}$, and a rabbit anti-DBH antibody (1:50, Abcam, #ab209487) was used to label adrenergic terminals in the hippocampus. Alexa-488-conjugated goat-anti-chicken and Alexa-555-conjugated goat-anti-rabbit secondary antibodies were used as the secondary antibody, and the nuclei were counterstained with DAPI. The sections were imaged using a confocal microscope (Nikon).

Fluorescence imaging of zebrafish

Tg(HuC:GRAB-NE_{1m}) zebrafish larvae were imaged by using an upright confocal microscope (Olympus FV1000, Japan) equipped with a 20x water-dipping objective (0.95 NA). The larvae were first paralyzed with α-bungarotoxin (100 μg/ml, Sigma), mounted dorsal side up in 1.5% low melting-point agarose (Sigma), and then perfused with an extracellular solution consisting of (in mM) 134 NaCl, 2.9 KCl, 4 $CaCl_2$, 10 HEPES, and 10 glucose (290 mOsmol/L, pH 7.8). Images were acquired at 1-2 Hz with a view field of 800 × 800 pixels and a voxel size was 0.62 × 0.62 × 2.0 μm^3 (x × y × z). To detect the sensor's response to exogenous NE, 50 μM L-(-)-norepinephrine (+)-bitartrate salt monohydrate (Sigma) in 5 μM L-ascorbic acid and 50 μM yohimbine hydrochloride (TOCRIS) were sequentially applied to the bath. To detect endogenous NE release, visual looming stimuli, which mimic approaching objects or predators (Yao et al., 2016) were projected to the larvae under a red background. Each trial lasted 5 s, and 5 trials were performed in a block, with a 90-s interval between trials. To examine the specificity of responses, ICI 118,551 hydrochloride (50 μM, Sigma) and desipramine hydrochloride (50 μM, Sigma) were applied. Looming stimuli in transiently transfected

HuC:GRAB$_{NE1m}$ zebrafish were measured at single-cell resolution by using the same conditions described above.

Fiber photometry recording in freely moving mice during optical stimulation

In the all-optic experiments shown in Figure 6, multimode optical fiber probes (105/125 μm core/cladding) were implanted into the LC (AP: -5.45 mm relative to Bregma; ML: ±0.85 mm relative to Bregma; and DV: -3.5 mm from the brain surface) and the SNc (AP: -3.1 mm relative to Bregma; ML: ±1.5 mm relative to Bregma; and DV: -3.85 mm from the brain surface) in mice four weeks after viral injection. Fiber photometry recording in the LC and/or SNc was performed using a 473-nm laser with an output power of 25 μW measured at the end of the fiber. The measured emission spectra were fitted using a linear unmixing algorithm (https://www.niehs.nih.gov/research/atniehs/labs/ln/pi/iv/tools/index.cfm). The coefficients generated by the unmixing algorithm were used to represent the fluorescence intensities of various fluorophores (Meng et al., 2018). To evoke C1V1-mediated NE/DA release, pulse trains (10-ms pulses at 20 Hz for 1 s) were delivered to the LC/SNc using a 561-nm laser with an output power of 9.9 mW measured at the end of the fiber.

Fiber photometry recording in mice during behavioral testing

For the experiments in Figure 7, a fiber photometry recording set-up was generated and used as previously described (Falkner et al., 2016). GRAB$_{NE1m}$ was injected into the lateral hypothalamus (Bregma AP: -1.7mm; ML: 0.90 mm DV: -4.80 mm) of C57BL/6 mice in a volume of 100 nl containing AAV9-hSyn-GRAB$_{NE1m}$ (Vigene, 1x10^{13} titer genomic copies per ml) at 10 nl/min. A 400-μm optic fiber (Thorlabs, BFH48-400) housed in a ceramic ferrule (Thorlabs, SFLC440-10) was implanted 0.2 mm above the injection site. The virus was left to incubate for three weeks. Prior to fiber photometry recording, a ferrule sleeve was used to connect a matching optic fiber to the implanted fiber. For recordings, a 400-Hz sinusoidal blue LED light (30 μW; M470F1 driven by an LEDD1B driver; both from Thorlabs) was bandpass-filtered (passing band: 472 ± 15 nm, Semrock, FF02-472/30-25) and delivered to the brain in order to excite GRAB$_{NE1m}$. The emission light passed through the same optic fiber, through a bandpass filter (passing band: 534 ± 25 nm, Semrock, FF01-535/50), and into a Femtowatt Silicon Photoreceiver, which recorded the GRAB$_{NE1m}$ emission using an RZ5 real-time processor (Tucker-Davis Technologies). The 400-Hz signals from the photoreceiver were extracted in real time using a custom program (Tucker-Davis Technologies) and used to reflect the intensity of the GRAB$_{NE1m}$ fluorescence signal.

Behavioral assays

All behavioral tests were performed at least one hour after the onset of the dark cycle. For the tail suspension test, each mouse was gripped by the tail and lifted off the bottom of its cage six times for 60 s each, with at least one minute between each lift. For the forced swim test, the mouse was gently placed in a 1000-ml conical flask containing lukewarm water and removed after 4-6 minutes. After removal from the water, the mouse was gently

dried with paper towels and placed in the home cage on a heating pad. For conspecific assays, an adult C57BL/6 group-housed mouse of either sex was placed inside the test mouse's cage for 10 minutes. No sexual behavior or aggressive behavior was observed during the interaction. For the food assay, ~4g of peanut butter was placed in the cap of a 15-ml plastic tube and placed inside of the test mouse's cage for 10 minutes. During that period, the test mouse was free to explore, sniff, and eat the peanut butter. All videos were acquired at 25 frames per second and manually annotated frame-by-frame using a custom MATLAB program (Lin et al., 2011). "Contact" with the social stimulus refers to the period in which the test mouse sniffed or was sniffed by the intruder. "Contact" with the peanut butter refers to the period in which the test mouse sniffed or ate the peanut butter. "Lift" refers to the period in which the experimenter gripped the mouse's tail and lifted the mouse into the air.

Quantification and statistical analysis

For the imaging experiments using cultured HEK293T cells, primary neurons, and brain slices, images were first imported to ImageJ software (National Institutes of Health) for fluorescence intensity readouts, and then analyzed using MATLAB (MathWorks) with a custom-written script or Origin Pro (OriginLab). The fluorescence response traces in the brain slices shown in Figure 4 were processed with 3x binning and then plotted.

Time-lapse images of the zebrafish were analyzed using Fiji to acquire the fluorescence intensity in the region of interest (ROI) in each frame. A custom-written MATLAB program was then used to calculate the change in fluorescence intensity ($\Delta F/F_0$) as follows: $\Delta F/F_0=(F_t-F_0)/F_0$, where F_t was the fluorescence intensity at time t and F_0 was the average fluorescence intensity during the entire time window. Statistical analyses were performed using GraphPad Prism 6 and Origin Pro (OriginLab).

For the fiber photometry data shown in Figure 7, the MATLAB function "msbackadj" with a moving window of 25% of the total recording duration was first applied to obtain the instantaneous baseline signal ($F_{baseline}$). The instantaneous $\Delta F/F$ was calculated as $(F_{raw} - F_{baseline})/F_{baseline}$, and a peri-stimulus histogram (PSTH) was calculated by aligning the $\Delta F/F$ signal of each trial to the onset of the behavior of interest. The response elicited during a behavior was calculated as the average $\Delta F/F$ during all trials of a given behavior. The response between behavioral periods was calculated as the average $\Delta F/F$ between two behavioral episodes excluding 4 s immediately before the behavior's onset, as some uncontrolled and/or unintended events (e.g., chasing the animal before the tail suspension test) may have occurred during that period. The baseline signal was calculated as the average $\Delta F/F$ 100 s prior to the start of the behavioral test. The peak response after each drug injection was calculated as the average maximum $\Delta F/F$ during all tail suspension trials. The decay time was calculated as the average time required to reach half of the peak response.

Except where indicated otherwise, group differences were analyzed using the Student's *t*-test, Wilcoxon matched-pairs signed rank test, Shapiro-Wilk normality test, one-way ANOVA test, or Friedman's test. Except where indicated otherwise, all summary data are presented as the mean ± SEM.

Data and software availability

The custom MATLAB programs using in this study will be provided upon request to the corresponding author.

References

Akerboom, J., Chen, T.-W., Wardill, T.J., Tian, L., Marvin, J.S., Mutlu, S., Calderón, N.C., Esposti, F., Borghuis, B.G., Sun, X.R., *et al.* (2012). Optimization of a GCaMP Calcium Indicator for Neural Activity Imaging. The Journal of Neuroscience *32*, 13819.

Bast, N., Poustka, L., and Freitag, C.M. (2018). The locus coeruleus-norepinephrine system as pacemaker of attention - a developmental mechanism of derailed attentional function in autism spectrum disorder. Eur J Neurosci *47*, 115-125.

Berridge, C.W., Schmeichel, B.E., and Espana, R.A. (2012). Noradrenergic modulation of wakefulness/arousal. Sleep Med Rev *16*, 187-197.

Berridge, C.W., and Spencer, R.C. (2016). Differential cognitive actions of norepinephrine a2 and a1 receptor signaling in the prefrontal cortex. Brain Res *1641*, 189-196.

Berridge, C.W., and Waterhouse, B.D. (2003). The locus coeruleus–noradrenergic system: modulation of behavioral state and state-dependent cognitive processes. Brain Research Reviews *42*, 33-84.

Bito, L., Davson, H., Levin, E., Murray, M., and Snider, N. (1966). THE CONCENTRATIONS OF FREE AMINO ACIDS AND OTHER ELECTROLYTES IN CEREBROSPINAL FLUID, IN VIVO DIALYSATE OF BRAIN, AND BLOOD PLASMA OF THE DOG*. Journal of Neurochemistry *13*, 1057-1067.

Brodde, O.-E., Bruck, H., Leineweber, K., and Seyfarth, T. (2001). Presence, distribution and physiological function of adrenergic and muscarinic receptor subtypes in the human heart. Basic Research in Cardiology *96*, 528-538.

Bruns, D. (2004). Detection of transmitter release with carbon fiber electrodes. Methods *33*, 312-321.

Chefer, V.I., Thompson, A.C., Zapata, A., and Shippenberg, T.S. (2009). Overview of Brain Microdialysis. Current Protocols in Neuroscience *47*, 7.1.1-7.1.28.

Chrousos, G.P. (2009). Stress and disorders of the stress system. Nat Rev Endocrinol *5*, 374-381.

Chung, K.Y., Rasmussen, S.G., Liu, T., Li, S., DeVree, B.T., Chae, P.S., Calinski, D., Kobilka, B.K., Woods, V.L., Jr., and Sunahara, R.K. (2011). Conformational changes in the G protein Gs induced by the beta2 adrenergic receptor. Nature *477*, 611-615.

Espay, A.J., LeWitt, P.A., and Kaufmann, H. (2014). Norepinephrine deficiency in Parkinson's disease: the case for noradrenergic enhancement. Mov Disord *29*, 1710-1719.

Falkner, A.L., Grosenick, L., Davidson, T.J., Deisseroth, K., and Lin, D. (2016). Hypothalamic control of male aggression-seeking behavior. Nature Neuroscience *19*, 596.

Fenno, L., Yizhar, O., and Deisseroth, K. (2011). The development and application of optogenetics. Annu Rev Neurosci *34*, 389-412.

Goddard, A.W., Ball, S.G., Martinez, J., Robinson, M.J., Yang, C.R., Russell, J.M., and Shekhar, A. (2010). Current perspectives of the roles of the central norepinephrine system in anxiety and depression. Depress Anxiety *27*, 339-350.

Hashikawa, K., Hashikawa, Y., Falkner, A., and Lin, D. (2016). The neural circuits of mating and fighting in male mice. Current opinion in neurobiology *38*, 27-37.

Inoue, A., Ishiguro, J., Kitamura, H., Arima, N., Okutani, M., Shuto, A., Higashiyama, S., Ohwada, T., Arai, H., Makide, K., *et al.* (2012). TGFα shedding assay: an accurate and versatile method for detecting GPCR activation. Nature Methods *9*, 1021.

Jing, M., Zhang, P., Wang, G., Feng, J., Mesik, L., Zeng, J., Jiang, H., Wang, S., Looby, J.C., Guagliardo, N.A., *et al.* (2018). A genetically encoded fluorescent acetylcholine indicator for in vitro and in vivo

studies. Nature Biotechnology *36*, 726.

Justice, J.B. (1993). Quantitative microdialysis of neurotransmitters. Journal of Neuroscience Methods *48*, 263-276.

Kroeze, W.K., Sassano, M.F., Huang, X.-P., Lansu, K., McCorvy, J.D., Giguère, P.M., Sciaky, N., and Roth, B.L. (2015). PRESTO-Tango as an open-source resource for interrogation of the druggable human GPCRome. Nature Structural &Amp; Molecular Biology *22*, 362.

Lee, G.J., Park, J.H., and Park, H.K. (2008). Microdialysis applications in neuroscience. Neurological Research *30*, 661-668.

Leibowitz, S.F. (1970). Reciprocal Hunger-Regulating Circuits Involving Alpha-and Beta-Adrenergic Receptors Located, Respectively, in the Ventromedial and Lateral Hypothalamus. Proceedings of the National Academy of Sciences of the United States of America *67*, 1063-1070.

Leibowitz, S.F., Jhanwar-Uniyal, M., Dvorkin, B., and Makman, M.H. (1982). Distribution of α-adrenergic, β-adrenergic and dopaminergic receptors in discrete hypothalamic areas of rat. Brain Research *233*, 97-114.

Li, L., Feng, X., Zhou, Z., Zhang, H., Shi, Q., Lei, Z., Shen, P., Yang, Q., Zhao, B., Chen, S.*, et al.* (2018). Stress Accelerates Defensive Responses to Looming in Mice and Involves a Locus Coeruleus-Superior Colliculus Projection. Curr Biol *28*, 859-871 e855.

Manglik, A., Kim, T.H., Masureel, M., Altenbach, C., Yang, Z., Hilger, D., Lerch, M.T., Kobilka, T.S., Thian, F.S., Hubbell, W.L.*, et al.* (2015). Structural Insights into the Dynamic Process of beta2-Adrenergic Receptor Signaling. Cell *161*, 1101-1111.

Marien, M.R., Colpaert, F.C., and Rosenquist, A.C. (2004). Noradrenergic mechanisms in neurodegenerative diseases: a theory. Brain Research Reviews *45*, 38-78.

Marvin, J.S., Borghuis, B.G., Tian, L., Cichon, J., Harnett, M.T., Akerboom, J., Gordus, A., Renninger, S.L., Chen, T.W., Bargmann, C.I.*, et al.* (2013). An optimized fluorescent probe for visualizing glutamate neurotransmission. Nat Methods *10*, 162-170.

McQuade, R., and Stanford, S.C. (2000). A microdialysis study of the noradrenergic response in rat frontal cortex and hypothalamus to a conditioned cue for aversive, naturalistic environmental stimuli. Psychopharmacology *148*, 201-208.

Meng, C., Zhou, J., Papaneri, A., Peddada, T., Xu, K., and Cui, G. (2018). Spectrally Resolved Fiber Photometry for Multi-component Analysis of Brain Circuits. Neuron *98*, 707-717.e704.

Moore, R.Y., and Bloom, F.E. (1979). Central Catecholamine Neuron Systems: Anatomy and Physiology of the Norepinephrine and Epinephrine Systems. Annual Review of Neuroscience *2*, 113-168.

Moret, C., and Briley, M. (2011). The importance of norepinephrine in depression. Neuropsychiatr Dis Treat *7*, 9-13.

Muller, A., Joseph, V., Slesinger, P.A., and Kleinfeld, D. (2014). Cell-based reporters reveal in vivo dynamics of dopamine and norepinephrine release in murine cortex. Nature Methods *11*, 1245.

Nakanishi, J., Takarada, T., Yunoki, S., Kikuchi, Y., and Maeda, M. (2006). FRET-based monitoring of conformational change of the β2 adrenergic receptor in living cells. Biochemical and Biophysical Research Communications *343*, 1191-1196.

Nygaard, R., Zou, Y., Dror, R.O., Mildorf, T.J., Arlow, D.H., Manglik, A., Pan, A.C., Liu, C.W., Fung, J.J., Bokoch, M.P.*, et al.* (2013). The dynamic process of beta(2)-adrenergic receptor activation. Cell *152*, 532-542.

Olive, M.F., Mehmert, K.K., and Hodge, C.W. (2000). Microdialysis in the mouse nucleus accumbens:

a method for detection of monoamine and amino acid neurotransmitters with simultaneous assessment of locomotor activity. Brain Research Protocols *5*, 16-24.

Pacak, K., Palkovits, M., Kopin, I.J., and Goldstein, D.S. (1995). Stress-Induced Norepinephrine Release in the Hypothalamic Paraventricular Nucleus and Pituitary-Adrenocortical and Sympathoadrenal Activity: In Vivo Microdialysis Studies. Frontiers in Neuroendocrinology *16*, 89-150.

Park, J., Kile, B.M., and Mark Wightman, R. (2009). In vivo voltammetric monitoring of norepinephrine release in the rat ventral bed nucleus of the stria terminalis and anteroventral thalamic nucleus. European Journal of Neuroscience *30*, 2121-2133.

Patriarchi, T., Cho, J.R., Merten, K., Howe, M.W., Marley, A., Xiong, W.-H., Folk, R.W., Broussard, G.J., Liang, R., Jang, M.J.*, et al.* (2018). Ultrafast neuronal imaging of dopamine dynamics with designed genetically encoded sensors. Science *360*.

Rasmussen, S.G., Choi, H.J., Fung, J.J., Pardon, E., Casarosa, P., Chae, P.S., Devree, B.T., Rosenbaum, D.M., Thian, F.S., Kobilka, T.S.*, et al.* (2011a). Structure of a nanobody-stabilized active state of the beta(2) adrenoceptor. Nature *469*, 175-180.

Rasmussen, S.G., DeVree, B.T., Zou, Y., Kruse, A.C., Chung, K.Y., Kobilka, T.S., Thian, F.S., Chae, P.S., Pardon, E., Calinski, D.*, et al.* (2011b). Crystal structure of the beta2 adrenergic receptor-Gs protein complex. Nature *477*, 549-555.

Ren, Q., Kurose, H., Lefkowitz, R.J., and Cotecchia, S. (1993). Constitutively active mutants of the alpha 2-adrenergic receptor. Journal of Biological Chemistry *268*, 16483-16487.

Robinson, D.L., Hermans, A., Seipel, A.T., and Wightman, R.M. (2008). Monitoring Rapid Chemical Communication in the Brain. Chemical Reviews *108*, 2554-2584.

Robinson, D.L., Venton, B.J., Heien, M.L.A.V., and Wightman, R.M. (2003). Detecting Subsecond Dopamine Release with Fast-Scan Cyclic Voltammetry in Vivo. Clinical Chemistry *49*, 1763.

Schwarz, L.A., and Luo, L. (2015). Organization of the Locus Coeruleus-Norepinephrine System. Current Biology *25*, R1051-R1056.

Schwarz, L.A., Miyamichi, K., Gao, X.J., Beier, K.T., Weissbourd, B., DeLoach, K.E., Ren, J., Ibanes, S., Malenka, R.C., Kremer, E.J.*, et al.* (2015). Viral-genetic tracing of the input–output organization of a central noradrenaline circuit. Nature *524*, 88.

Shekhar, A., Katner, J.S., Sajdyk, T.J., and Kohl, R.R. (2002). Role of norepinephrine in the dorsomedial hypothalamic panic response: An in vivo microdialysis study. Pharmacology Biochemistry and Behavior *71*, 493-500.

Singleman, C., and Holtzman, N.G. (2014). Growth and Maturation in the Zebrafish, Danio Rerio: A Staging Tool for Teaching and Research. Zebrafish *11*, 396-406.

Sokolowski, K., and Corbin, J.G. (2012). Wired for behaviors: from development to function of innate limbic system circuitry. Frontiers in Molecular Neuroscience *5*, 55.

Sun, F., Zeng, J., Jing, M., Zhou, J., Feng, J., Owen, S.F., Luo, Y., Li, F., Wang, H., Yamaguchi, T.*, et al.* (2018). A Genetically Encoded Fluorescent Sensor Enables Rapid and Specific Detection of Dopamine in Flies, Fish, and Mice. Cell *174*, 481-496.e419.

Tanaka, M. (1999). Emotional Stress and Characteristics of Brain Noradrenaline Release in the Rat. INDUSTRIAL HEALTH *37*, 143-156.

Urban, D.J., and Roth, B.L. (2015). DREADDs (designer receptors exclusively activated by designer drugs): chemogenetic tools with therapeutic utility. Annu Rev Pharmacol Toxicol *55*, 399-417.

Vilardaga, J.-P., Bünemann, M., Krasel, C., Castro, M., and Lohse, M.J. (2003). Measurement of the

millisecond activation switch of G protein–coupled receptors in living cells. Nature Biotechnology *21*, 807.

Wan, Q., Okashah, N., Inoue, A., Nehmé, R., Carpenter, B., Tate, C.G., and Lambert, N.A. (2018). Mini G protein probes for active G protein-coupled receptors (GPCRs) in live cells. Journal of Biological Chemistry.

Wang, A., Feng, J., Li, Y., and Zou, P. (2018a). Beyond Fluorescent Proteins: Hybrid and Bioluminescent Indicators for Imaging Neural Activities. ACS Chemical Neuroscience *9*, 639-650.

Wang, H., Jing, M., and Li, Y. (2018b). Lighting up the brain: genetically encoded fluorescent sensors for imaging neurotransmitters and neuromodulators. Curr Opin Neurobiol *50*, 171-178.

Watson, C.J., Venton, B.J., and Kennedy, R.T. (2006). In Vivo Measurements of Neurotransmitters by Microdialysis Sampling. Analytical Chemistry *78*, 1391-1399.

Yang, T., and Shah, N.M. (2016). Molecular and neural control of sexually dimorphic social behaviors. Current Opinion in Neurobiology *38*, 89-95.

Yao, Y., Li, X., Zhang, B., Yin, C., Liu, Y., Chen, W., Zeng, S., and Du, J. (2016). Visual Cue-Discriminative Dopaminergic Control of Visuomotor Transformation and Behavior Selection. Neuron *89*, 598-612.

Zhao, Y., Araki, S., Wu, J., Teramoto, T., Chang, Y.-F., Nakano, M., Abdelfattah, A.S., Fujiwara, M., Ishihara, T., Nagai, T*., et al.* (2011). An Expanded Palette of Genetically Encoded Ca(2+) Indicators. Science (New York, NY) *333*, 1888-1891.

Zhou, Z., and Misler, S. (1995). Amperometric detection of stimulus-induced quantal release of catecholamines from cultured superior cervical ganglion neurons. Proceedings of the National Academy of Sciences *92*, 6938.

Zimmerman, B.G. (1981). Adrenergic Facilitation by Angiotensin: Does it Serve a Physiological Function? Clinical Science *60*, 343.

Zou, P., Zhao, Y., Douglass, A.D., Hochbaum, D.R., Brinks, D., Werley, C.A., Harrison, D.J., Campbell, R.E., and Cohen, A.E. (2014). Bright and fast multicoloured voltage reporters via electrochromic FRET. Nat Commun *5*, 4625.

Figure 1. Design and optimization of genetically encoded NE sensors.

(**A**) Selection of a candidate sensor scaffold by screening several NE-binding GPCRs. Shown at the right are example images of the indicated chimeric GPCR-cpEGFP candidates expressed in HEK293T cells. Yellow arrows indicate robust membrane trafficking, and red arrows indicate impaired membrane trafficking. See also Figure S1.

(**B**) Identification of the most responsive NE sensor, NE0.5m (indicated by the black square) by screening the cpEGFP insertion site in ICL3 of the α2AR. $\Delta F/F_0$ refers to the peak change in fluorescence intensity in response to 100 μM NE.

(**C**) Optimizing the $GRAB_{NE}$ sensors by mutational screening of the insertion linker. NE0.5m was used as a template, and the indicated amino acids on N-terminal and C-terminal sides of the cpEGFP insert were mutated individually. Sensor NE1m (indicated by the pink squares) was identified due to having the strongest response ($\Delta F/F_0$) and brightness relative to the original NE0.5m sensor (indicated by the dashed line at 1.0).

(**D**) Tuning the sensor's affinity for NE by introducing mutations in the GPCR. Magnified views of the ligand-binding pocket view from the cytosol are shown; key residues involved in ligand binding and inducing a conformational change upon ligand binding are indicated. The middle panel shows example images of HEK293T cells expressing the indicated $GRAB_{NE}$ sensors; EGFP fluorescence is shown in the left column, and the fluorescence response in the presence of 100 μM NE is shown in the right column. Shown at the right are the normalized dose-response curves for the three $GRAB_{NE}$ sensors, with C_{50} values (top), and the average fluorescence change in response to 100 μM NE (bottom); n = 21-67 cells from 3-5 cultures for each sensor.

The scale bars in (A) and (D) represent 10 μm.

***$p < 0.001$ (Student's *t*-test).

Figure 2. Characterization of $GRAB_{NE}$ sensors in cultured cells.

(**A-C**) HEK293T cells were loaded with NPEC-NE, which was uncaged by photolysis with a pulse of 405-nm light. Uncaging caused a rapid increase in $GRAB_{NE1h}$ fluorescence, which was blocked in the presence of 10 μM yohimbine (YO). The data in A represent 3 trials each, and the data in C represent 7 cells from 3 cultures. The white dotted square indicates the image region and the purple square indicates the illumination region.

(**D-F**) NE was applied to HEK293T cells expressing $GRAB_{NE1m}$ or $GRAB_{NE1h}$ to measure τ_{on}. Yohimbine (YO) was then applied in order to measure τ_{off}; The white dotted line indicates the line-scanning region. n ≥ 6 cells from 6 cultures.

(**G**) The indicated compounds were applied to $GRAB_{NE1m}$ and $GRAB_{NE1h}$, and the change in fluorescence relative to NE is plotted.

(**H**) Dose-response curves for $GRAB_{NE1m}$, $GRAB_{NE1h}$, and wild-type α2AR for NE and DA, with EC_{50} values shown; n ≥ 3 wells with 100-300 cells each.

(**I**) Fast-scan cyclic voltammetry measurements in response to increasing concentrations of NE and DA. The insets show exemplar cyclic voltammograms of NE and DA at 100 μM, with peak current occurring at ~0.6 V.

(**J**) Time course of $\Delta F/F_0$ for $GRAB_{NE}$ sensors measured over a 2-h time frame; note that the fluorescent signal remained at the cell surface even after 180 min, indicating no measurable internalization or desensitization. n = 3 wells with 100-300 cells each.

(**K**) A TANGO assay was performed in order to measure β-arrestin–mediated signaling by $GRAB_{NE1m}$, $GRAB_{NE1h}$, and wild-type α2AR in the presence of increasing concentrations of NE; n = 4 wells with $\geq 10^5$ cells each.

(**L,M**) $GRAB_{NE}$ sensors do not couple to downstream G protein signaling pathways. Wild-type α2AR, but not $GRAB_{NE1m}$ or $GRAB_{NE1h}$, drives Gαi signaling measured using a luciferase complementation assay (L). Disrupting of G protein activation with pertussis toxin does not affect the NE-induced fluorescence change in $GRAB_{NE1m}$ or $GRAB_{NE1h}$ (M). n = 3 wells with $\geq 10^5$ cells each.

The scale bars in (A), (D), and (J) represent 10 μm.

*$p < 0.05$, **$p < 0.01$, and ***$p < 0.001$; n.s., not significant (Student's *t*-test).

Figure 3. Characterization of $GRAB_{NE}$ sensors in cultured neurons.

(**A-C**) $GRAB_{NE1m}$ is expressed in various plasma membrane compartment of cultured neurons. Cultured cortical neurons were co-transfected with $GRAB_{NE1m}$ and RFP-CAAX to label the plasma membrane, and the fluorescence response induced by bath application of NE was measured in the cell body, dendritic shaft and spine, and axon (**C**). n > 10 neurons from 4 cultures.

(**D,E**) Cultured cortical neurons expressing $GRAB_{NE1m}$ and $GRAB_{NE1h}$, but not $GRAB_{NEmut}$, respond to application of NE (10 μM). EGFP fluorescence and pseudocolor images depicting the response to NE are shown in (**D**), and the time course and summary of peak $\Delta F/F_0$ are shown in (**E**). n > 15 neurons from 3 cultures.

(**F**) Dose-response curve for $GRAB_{NE}$ sensors expressed in cultured cortical neurons in response to NE and DA. n > 10 neurons from 3 cultures.

(**G**) Example trace (top) and summary (bottom) of cultured neurons transfected with $GRAB_{NE1m}$ and treated with the indicated compounds at 10 μM each. n = 9 neurons from 3 cultures.

(**H,I**) The fluorescence change in $GRAB_{NE1m}$ induced by 100 μM NE is stable for up to 1 h. Representative images taken at the indicated times are shown in (**H**). An example trace and summary data are shown in (**I**). Where indicated, 10 μM yohimbine (YO) was added. n = 11 neurons from 3 cultures.

The scale bars in (**A**) and (**B**) represent 10 μm; the scale bars in (**D**) and (**H**) represent 25 μm.

***p < 0.001; n.s., not significant (Student's *t*-test).

Figure 4. Release of endogenous NE measured in mouse brain slices.

(A) Left, schematic illustration of the slice experiments. An AAV expressing hSyn-NE1m was injected into the LC; two weeks later, acute brain slices were prepared and used for electric stimulation experiments. **Right**, exemplar 2-photon microscopy images showing the distribution of $GRAB_{NE1m}$ in the plasma membrane of LC neurons.

(**B**) **Left and middle**, representative pseudocolor images and corresponding fluorescence changes in $GRAB_{NE1m}$-expressing neurons in response to 2, 20, and 100 pulses delivered at 20 Hz. The ROI (50-μm diameter) for data analysis is indicated in the images. **Right**, summary of the peak fluorescence change in slices stimulated as indicated; n = 5 slices from 5 mice.

(**C**) Exemplar traces and summary data of $GRAB_{NE1m}$-expressing neurons in response to 20 electrical stimuli delivered at 20 Hz in ACSF, 4-AP (100 μM), or 4-AP with Cd^{2+} (100μM); n = 4 slices from 4 mice.

(**D**) Kinetic properties of the electrically evoked fluorescence responses in $GRAB_{NE1m}$-expressing LC neurons. **Left**, image showing a $GRAB_{NE1m}$-expressing LC neuron for line scan analysis (red dashed line). **Middle and right**, example trace and summary of the responses elicited in $GRAB_{NE1m}$-expressing neurons before, and after 10 pulses delivered at 100Hz; n = 4 slices from 4 mice.

(**E**) The norepinephrine transporter blocker desipramine (Desi, 10 μM; red) increases the effect of electrical stimuli (20 pulses at 20 Hz) or two trains of stimuli with a 1-s interval compared to ACSF (black traces). n = 5 slices from 5 mice.

(**F**) The fluorescence response in $GRAB_{NE1m}$-expressing neurons is stable. Eight stimuli (20 pulses at 20 Hz) were applied at 5-min intervals, and the response (normalized to the first train) is plotted against time. n = 5 slices from 5 mice.

(**G**) Traces and summary data of the fluorescence response measured in neurons expressing $GRAB_{NE1m}$, $GRAB_{NEmut}$, or $GRAB_{DA1m}$ in response to 20 pulses delivered at 20 Hz in the presence of ACSF or 20 μM YO; n = 3-7 slices from 3-7 mice.

(**H**) Traces and summary data of the fluorescence response measured in neurons expressing $GRAB_{NE1m}$ or $GRAB_{DA1m}$. Where indicated, 50 μM NE, 50 μM DA, 20 μM yohimbine (YO), and/or 20 μM haloperidol (Halo) was applied to the cells. n = 3-5 slices from 3-5 mice.

The scale bars represent 10 μm.

*$p < 0.05$, **$p < 0.01$, and ***$p < 0.001$; n.s., not significant (Student's *t*-test).

Figure 5. $GRAB_{NE1m}$ can be used to measure noradrenergic activity *in vivo* in transgenic zebrafish.

(**A**) *In vivo* confocal image of a Tg(HuC:$GRAB_{NE1m}$) zebrafish expressing $GRAB_{NE1m}$ in neurons driven by the HuC promoter. Larvae at 6 days post-fertilization were used.

(**B-D**) Bath application of NE (50 μM) but not DA (50 μM) elicits a significant increase in fluorescence in the tectal neuropil of Tg(HuC:$GRAB_{NE1m}$) zebrafish, but not in $GRAB_{NEmut}$ zebrafish, and this increase is blocked by YO (50 μM), but not ICI 118,551 (50 μM). n = 7.

(**E-H**) Visual looming stimuli evoke the release of endogenous NE in the midbrain of $GRAB_{NE1m}$ zebrafish, but not in $GRAB_{NEmut}$ zebrafish. The looming stimuli paradigm is shown in the left of (**E**). Where indicated, YO (50 μM) or ICI 118,551 (50 μM) was applied. Desipramine (Desi, 50 μM) application slowed the decay of looming-induced NE release (**H**). n = 6 for $GRAB_{NEmut}$ and n = 9 for the others.

(**I-K**) Single-cell labeling of $GRAB_{NE1m}$ in the midbrain of zebrafish larva (**I**), with looming-evoked responses shown in (**I** and **J**). The summary data for 6 labeled cells are shown in (**K**).

The scale bar shown in (**A, left**) represents 10 μm; the scale bars shown in (**A, right**), (**B**) and (**E**) represent 50 μm. The scale bar shown in (**I**) represents 5 μm.

*$p < 0.05$, **$p < 0.01$, ***$p < 0.001$, and ****$p < 0.0001$; n.s., not significant (Wilcoxon matched-pairs signed rank test in panel **H**, all others were analyzed using the paired or unpaired Student's *t*-test).

Figure 6. $GRAB_{NE1m}$ can be used to measure optogenetically stimulated noradrenergic activity *in vivo* in freely moving mice.

(**A**) Schematic illustration depicting the experimental design for recording $GRAB_{NE1m}$ and $GRAB_{NEmut}$ fluorescence in response to optical stimulation of C1V1 in the locus coeruleus (LC).

(**B**) Representative traces of optogenetically stimulated $GRAB_{NE1m}$ (top) and $GRAB_{NEmut}$ (bottom) activity in the LC before (baseline, left), 15 min after an i.p. injection of the NET blocker desipramine (10 mg/kg, middle), and 15 min after an i.p. injection of the α2AR antagonist yohimbine (2 mg/kg, right). The vertical tick marks indicate the optogenetic stimuli. Black arrows represent the timing for grabbing and i.p. injection.

(**C-D**) Average traces of $GRAB_{NE1m}$ fluorescence (**C**), summary data (**D**), and the decay time constant (**E**) in response to optical stimulation in the LC following treatment with the indicated compounds. n = 15 trials from 3 mice for each condition.

(**F,G**) Schematic illustration (**F, left**), representative traces (**F, right**), average fluorescence change (**G, left**), and summary data (**G, right**) for $GRAB_{NE1m}$ in response to optical stimulation of noradrenergic neurons in the LC and dopaminergic neurons in the SNc.

***$p < 0.001$ (for D and E, One-Way ANOVA, for G, Student's *t*-test).

Figure 7. $GRAB_{NE1m}$ can be used to measure noradrenergic activity in the hypothalamus during stress, food-related behavior, and social interaction.

(**A**) Schematic diagrams depicting the fiber photometry recording, virus injection, and recording sites.

(**B**) Histology showing the expression of $GRAB_{NE1m}$ (green) and placement of the recording; the nuclei were counterstained with DAPI (blue). Scale bar: 500μm.

(**C1-E6**) Representative traces (**C1-C6**), average per-stimulus histograms (**D1-D6**), and summary data (**E1-E6**) showing normalized $GRAB_{NE1m}$ fluorescence (ΔF/F) before and during the forced swim test (**1**), the tail suspension test (**2**), the hand presentation test (**3**), social interaction with an intruder of the opposite sex (**4**) and the same sex (**5**), and presentation of peanut butter (**6**). n = 3 animals each.

(**F**) Representative traces of $GRAB_{NE1m}$ fluorescence during the tail suspension test 10 minutes after saline injection, 25 minutes after atomoxetine (ATX) or yohimbine (YO) injection, and 15 minutes after GBR 12909 or sulpiride (Sul) injection.

(**G-I**) Average peri-stimulus histograms (**H**), peak change in $GRAB_{NE1m}$ fluorescence, and post-test decay time measured during the tail suspension test after injection of the indicated compounds. n = 3 each.

The Shapiro-Wilk normality test was performed; if the test revealed that the followed a normal distribution, a paired Student's *t*-test or one-way repeated measures ANOVA followed by Tukey's multiple comparisons was performed. If the values did not follow a normal distribution, a non-parametric ANOVA (Friedman's test) was performed followed by Dunn's multiple comparisons test. In (**C**) and (**D**), the blue dotted lines represent the start of the stimulus, and the red dotted lines represent the end of the trial.

$^{*}p < 0.05$ and $^{**}p < 0.01$.

Figure S1. Characterization of the membrane trafficking of a panel of screening candidates (related to Fig. 1).

Representative images (**A**) of HEK293T cells co-transfected with the indicated screening candidates (green) together with RFP-CAAX (red) to label the plasma membrane. KDELR-EGFP was used as an ER marker. The dashed white lines indicate the line used for the line-scanning data shown in (**B**) and summarized in

(**C**) n = 30 cells from 4-5 cultures.

The scale bars in (**A**) represent 10 μm.

*$p < 0.05$ and ***$p < 0.001$; n.s., not significant (Student's *t*-test).

Figure S2. Further characterization of $GRAB_{NE}$ sensors (related to Fig. 2).

(**A**) Fluorescence intensity of $GRAB_{NE1m}$ and $GRAB_{NE1h}$ expressed relative to EGFP-α2AR. n ≥ 2 wells with 300-500 cells per well.

(**B**) G protein activation mediated by $GRAB_{NE1m}$ and wild-type α2AR was measured using the TGFα shedding assay and is expressed relative to α2AR. n = 4 wells with $\geq 10^5$ cells per well.

(**C**) Exemplar (**left**) and summary data (**right**) showing the photostability of $GRAB_{NE}$ sensors and EGFP-CAAX using confocal (**top**) and 2-photon (**bottom**) microscopy. n > 10 cells from at least 3 cultures.

(**D**) Exemplar cyclic voltammograms for 10 μM NE (**top**), 10 μM DA (**middle**), and 10 μM Glu (**bottom**) measured using FSCV are shown. The traces were averaged from separate 200 trials.

***$p < 0.001$ (Student's *t*-test).

Figure S3. $GRAB_{NE}$ sensors respond selectively to noradrenergic agonists in brain slices (related to Fig. 4).

(**A**) Schematic drawing showing the experimental design for measuring CA1 pyramidal neurons in cultured rat hippocampal slices.

(**B**) Heat-map images of the change in fluorescence in $GRAB_{NE1m}$-expressing CA1 neurons in response to a 10-ms local application of NE (20 μM). The red and orange traces show the fluorescence responses of two neurons, and the green trace shows the average response of all neurons in the field. The scale represents 20 μm.

(**C**) Fluorescence responses measured in $GRAB_{NE1m}$-, $GRAB_{NE1h}$-, and $GRAB_{NEmut}$-expressing CA1 neurons following a 10-ms puff (arrow) of ACSF, NE (20 μM), Epi (100 μM), or brimonidine (UK, 20 μM).

(**D**) Maximum $\Delta F/F_0$ response measured in $GRAB_{NE1m}$-, $GRAB_{NE1h}$-, and $GRAB_{NEmut}$-expressing CA1 neurons following a 10-ms puff of ACSF or NE. n = 20-21 cells from 8 animals per group.

(**E**) Rise times and decay time constants were measured in CA1 neurons expressing $GRAB_{NE1m}$- and $GRAB_{NE1h}$- expressing CA1 neurons in response to a puff of NE. n = 21 cells from 8 animals.

(**F**) Maximum $\Delta F/F_0$ response measured in $GRAB_{NE1m}$-expressing CA1 neurons following a puff of NE, Epi, or brimonidine (UK). n = 20-21 cells from 8 animals per group.

(**G**) Rise times and decay time constants were measured in $GRAB_{NE1m}$-expressing CA1 neurons following a puffs of Epi or brimonidine (UK).

(**H**) Schematic illustration depicting AAV-mediated delivery of $GRAB_{NE1h}$ in the mouse hippocampus and bath application of various agonists in the dentate gyrus.

(**I**) Example images showing $GRAB_{NE1h}$ (green) expression and dopamine beta hydroxylase (DBH) immunostaining (red) in the dentate gyrus of AAV-$GRAB_{NE1h}$- and control-injected hippocampi. The nuclei were counterstained with DAPI. The scale bar represents 100 μm.

(**J**) Electrical stimulation evokes NE release in the hippocampus measured as a change in $GRAB_{NE1h}$ fluorescence. The response was blocked by batch application of yohimbine (YO). Exemplar images (**left**), representative traces (**middle**), and the summary data (**right**) are shown.

(**K**) Normalized change in $GRAB_{NE1h}$ fluorescence in response to bath application of the indicated noradrenergic agonists in the presence or absence of ICI 118,551 or yohimbine.

The scale bar shown in (**B**) represents 20 μm; the scale bar shown in (**I**) represents 100 μm. The scale bar shown in (**J**) represents 10 μm.

*$p < 0.05$ and ***$p < 0.001$; n.s., not significant (Student's *t*-test, Wilcoxon test, or Mann-Whitney rank sum test).

Fig 1

A. Selection of NE sensitive GPCR

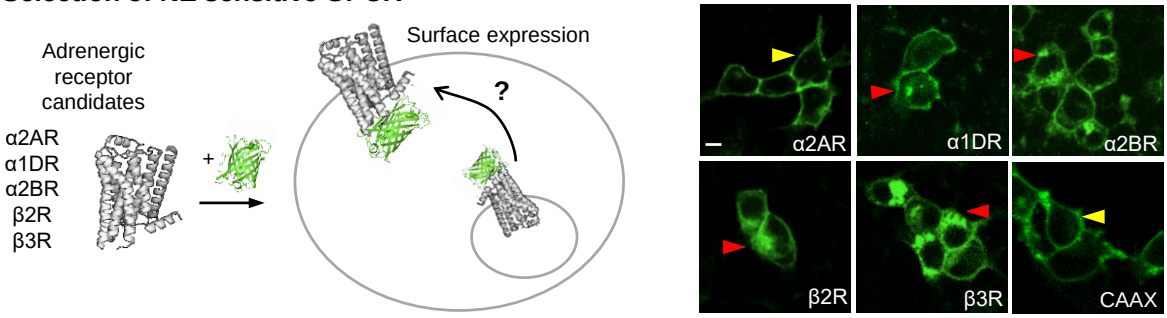

B. Insertion sites screening

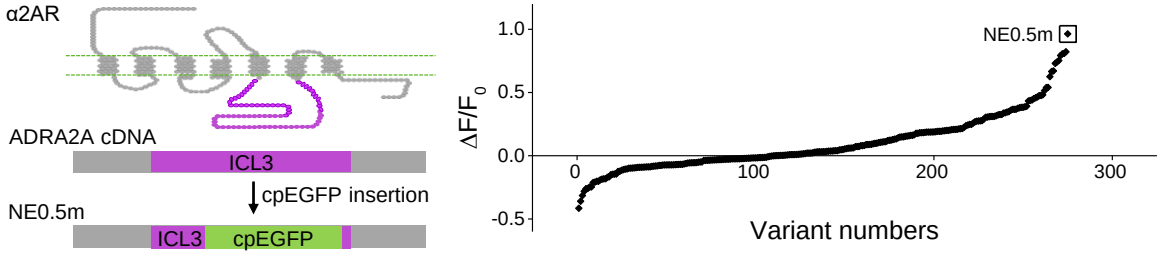

C. Optimization of coupling linkers

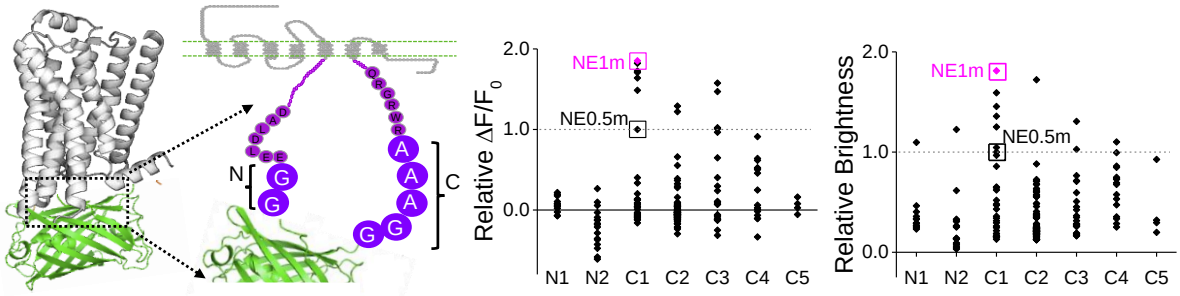

D. Affinity tuning of NE sensors

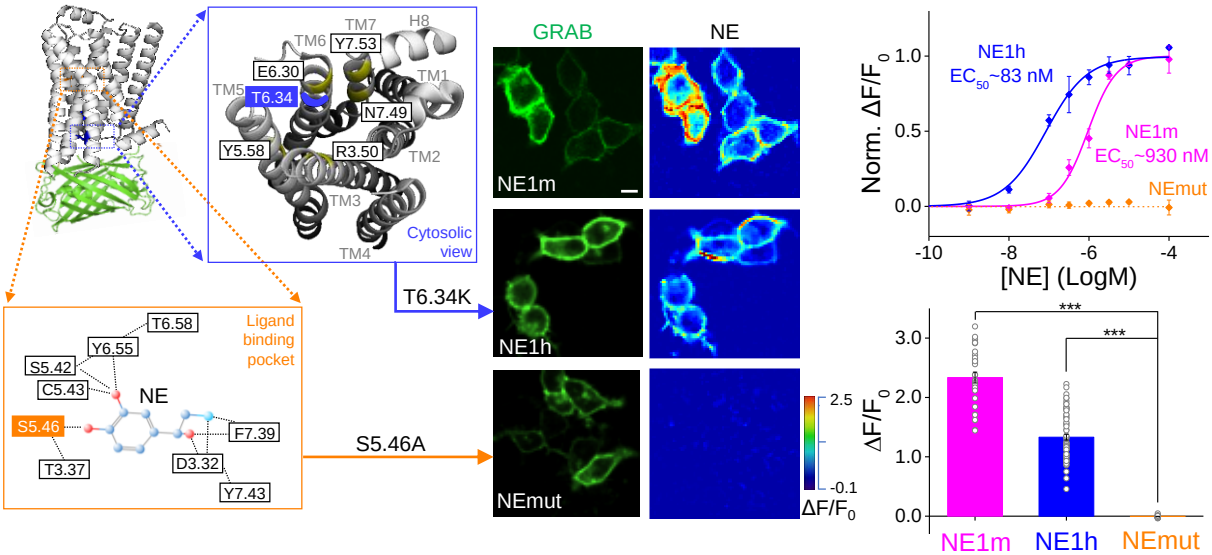

Fig 2

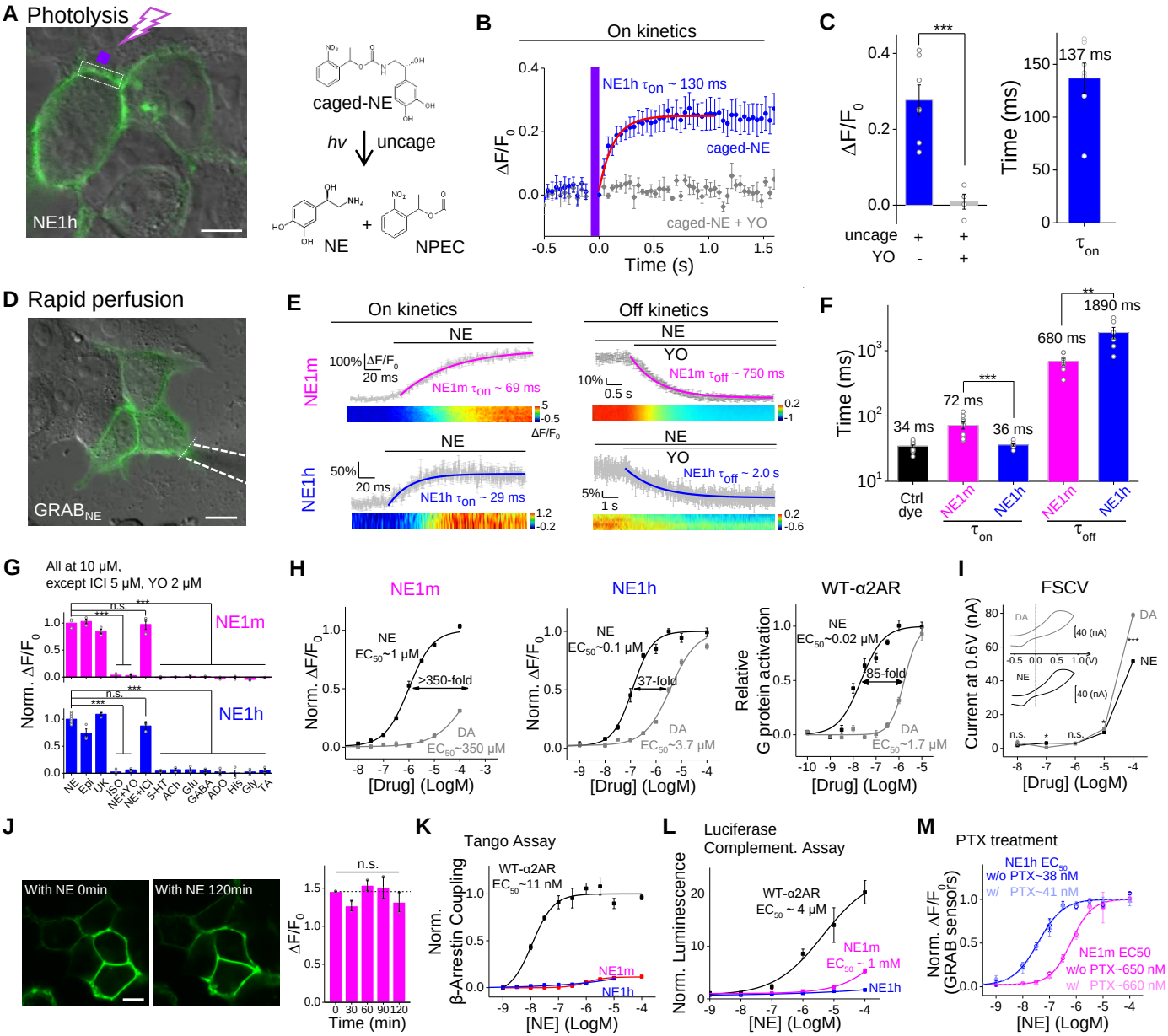
A Photolysis
NE1h
caged-NE
hv
uncage
NE
NPEC
B
On kinetics
NE1h τon ~ 130 ms
caged-NE
caged-NE + YO
ΔF/F0
Time (s)
C
***
ΔF/F0
uncage
YO
Time (ms)
137 ms
τon
D Rapid perfusion
GRABNE
E
On kinetics
Off kinetics
NE
YO
NE1m
NE1h
100% ΔF/F0
20 ms
NE1m τon ~ 69 ms
NE1m τoff ~ 750 ms
10%
0.5 s
50%
NE1h τon ~ 29 ms
NE1h τoff ~ 2.0 s
5%
1 s
ΔF/F0
F
Time (ms)
34 ms
72 ms
36 ms
680 ms
1890 ms
Ctrl dye
NE1m
NE1h
τon
τoff
G
All at 10 μM, except ICI 5 μM, YO 2 μM
Norm. ΔF/F0
n.s.
NE1m
NE1h
NE
Epi
UK
ISO
NE+YO
NE+ICI
5-HT
ACh
Gln
GABA
ADO
His
Gly
TA
H
NE1m
NE1h
WT-α2AR
NE
EC50~1 μM
>350-fold
DA
EC50~350 μM
EC50~0.1 μM
37-fold
EC50~3.7 μM
EC50~0.02 μM
85-fold
EC50~1.7 μM
Norm. ΔF/F0
Relative G protein activation
[Drug] (LogM)
I
FSCV
Current at 0.6V (nA)
DA
NE
40 (nA)
0.5 0.0 0.5 1.0 (V)
n.s.
[Drug] (LogM)
J
With NE 0min
With NE 120min
n.s.
ΔF/F0
Time (min)
K
Tango Assay
WT-α2AR
EC50~11 nM
NE1m
NE1h
Norm. β-Arrestin Coupling
[NE] (LogM)
L
Luciferase Complement. Assay
WT-α2AR
EC50 ~ 4 μM
NE1m
EC50 ~ 1 mM
NE1h
Norm. Luminescence
[NE] (LogM)
M
PTX treatment
NE1h EC50
w/o PTX~38 nM
w/ PTX~41 nM
NE1m EC50
w/o PTX~650 nM
w/ PTX~660 nM
Norm. ΔF/F0 (GRAB sensors)
[NE] (LogM)

Fig 3

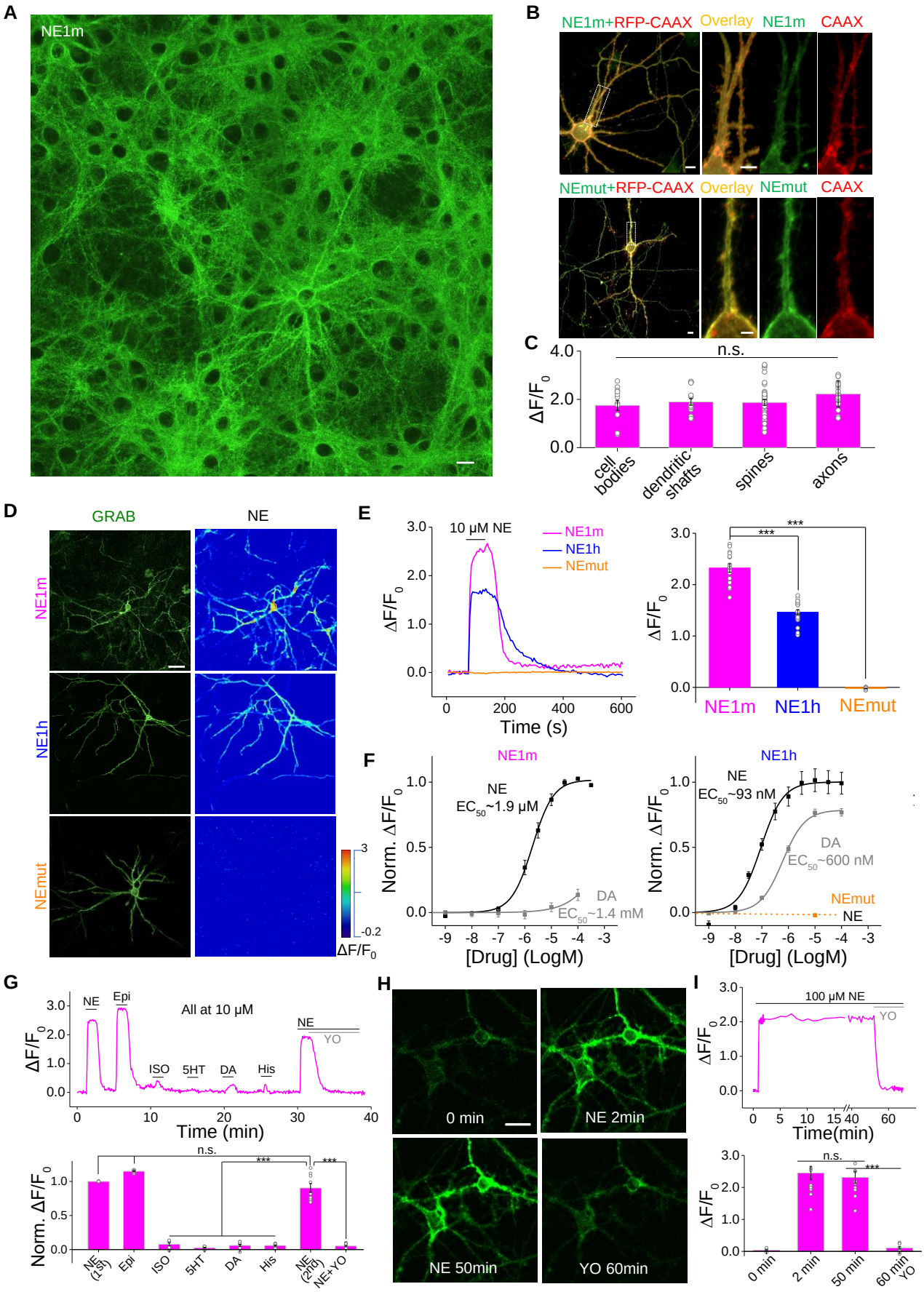
A
NE1m
B
NE1m+RFP-CAAX
Overlay
NE1m
CAAX
NEmut+RFP-CAAX
Overlay
NEmut
CAAX
C
n.s.
ΔF/F0
cell bodies
dendritic shafts
spines
axons
D
GRAB
NE
NE1m
NE1h
NEmut
ΔF/F0
E
10 μM NE
NE1m
NE1h
NEmut
Time (s)
***
F
NE1m
NE
EC50~1.9 μM
DA
EC50~1.4 mM
NE1h
EC50~93 nM
DA
EC50~600 nM
NEmut
NE
Norm. ΔF/F0
[Drug] (LogM)
G
All at 10 μM
NE
Epi
ISO
5HT
DA
His
YO
Time (min)
n.s.
***
NE (1st)
NE (2nd)
NE+YO
H
0 min
NE 2min
NE 50min
YO 60min
I
100 μM NE
YO
Time(min)
n.s.
0 min
2 min
50 min
60 min YO

Fig 4

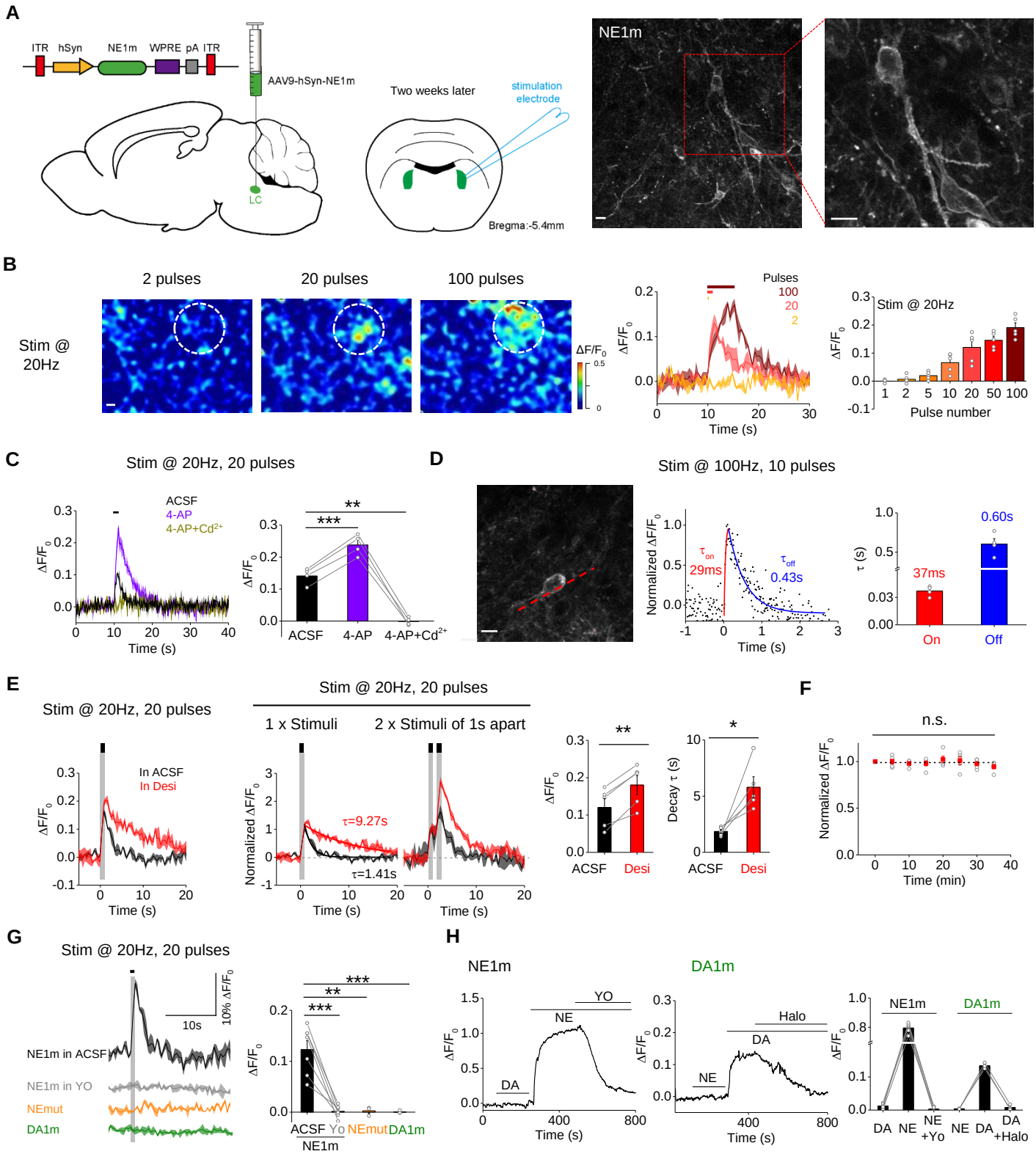
A
ITR hSyn NE1m WPRE pA ITR
AAV9-hSyn-NE1m
LC
Two weeks later
stimulation electrode
Bregma:-5.4mm
NE1m
B
2 pulses
20 pulses
100 pulses
Stim @ 20Hz
ΔF/F0
Pulses
100
20
2
Time (s)
Stim @ 20Hz
Pulse number
C
Stim @ 20Hz, 20 pulses
ACSF
4-AP
4-AP+Cd2+
Time (s)
D
Stim @ 100Hz, 10 pulses
Normalized ΔF/F0
τon
29ms
τoff
0.43s
τ (s)
37ms
0.60s
On
Off
E
Stim @ 20Hz, 20 pulses
In ACSF
In Desi
1 x Stimuli
2 x Stimuli of 1s apart
τ=9.27s
τ=1.41s
Decay τ (s)
ACSF
Desi
F
n.s.
Time (min)
G
Stim @ 20Hz, 20 pulses
10s
10% ΔF/F0
NE1m in ACSF
NE1m in YO
NEmut
DA1m
ACSF Yo NEmut DA1m
NE1m
H
NE1m
DA1m
YO
NE
DA
Halo
NE +Yo
DA +Halo

Fig 5

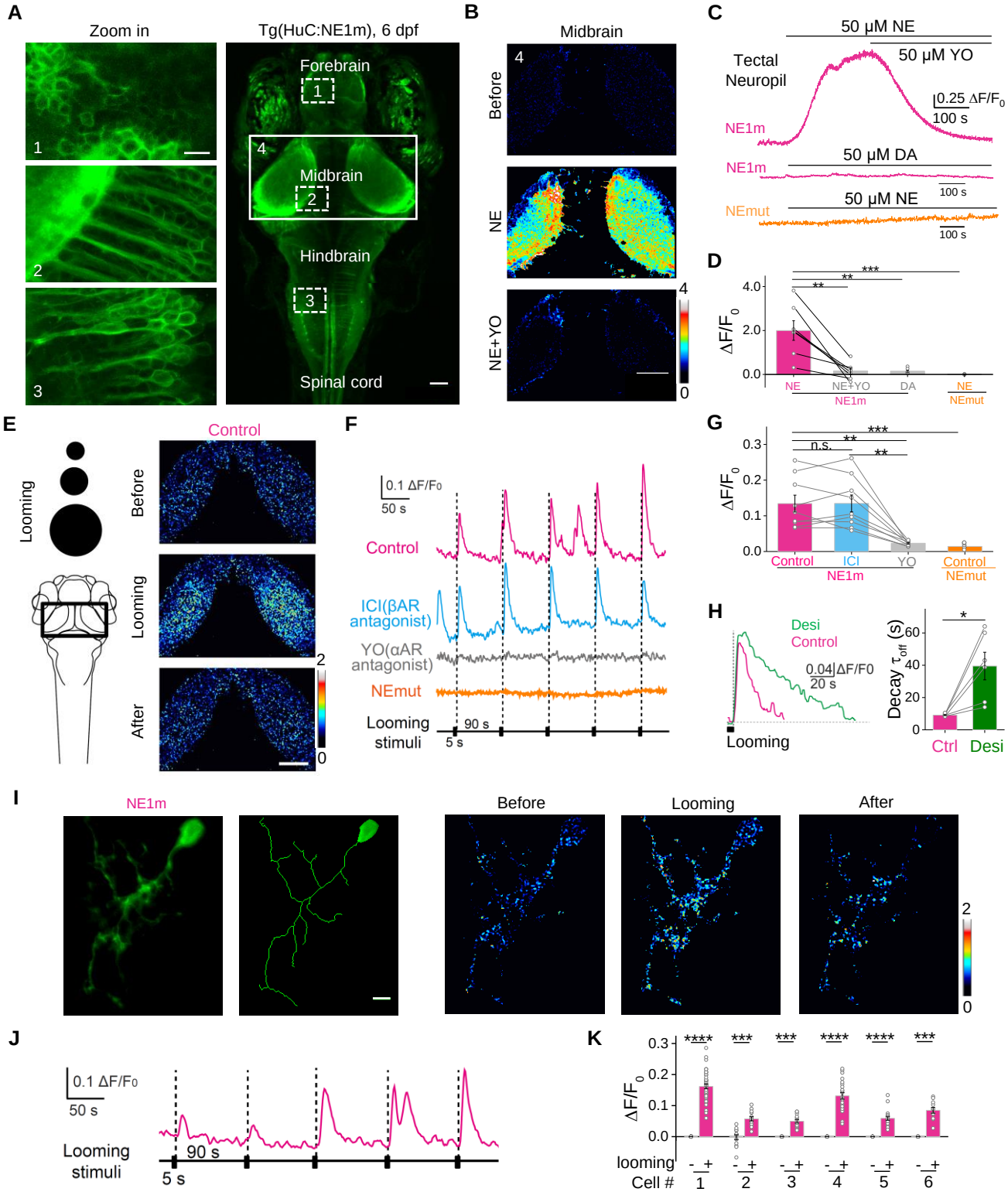
A
Zoom in
Tg(HuC:NE1m), 6 dpf
Forebrain
Midbrain
Hindbrain
Spinal cord
B
Midbrain
Before
NE
NE+YO
C
50 μM NE
50 μM YO
Tectal Neuropil
0.25 ΔF/F0
100 s
NE1m
50 μM DA
NEmut
D
ΔF/F0
NE
NE+YO
DA
NE1m
NEmut
E
Looming
Control
Before
Looming
After
F
0.1 ΔF/F0
50 s
Control
ICI(βAR antagonist)
YO(αAR antagonist)
NEmut
Looming stimuli
90 s
5 s
G
ΔF/F0
n.s.
Control
ICI
YO
NE1m
NEmut
H
Desi
Control
0.04 ΔF/F0
20 s
Looming
Decay τoff (s)
Ctrl
Desi
I
NE1m
Before
Looming
After
J
0.1 ΔF/F0
50 s
Looming stimuli
90 s
5 s
K
ΔF/F0
looming
Cell #

Fig 6

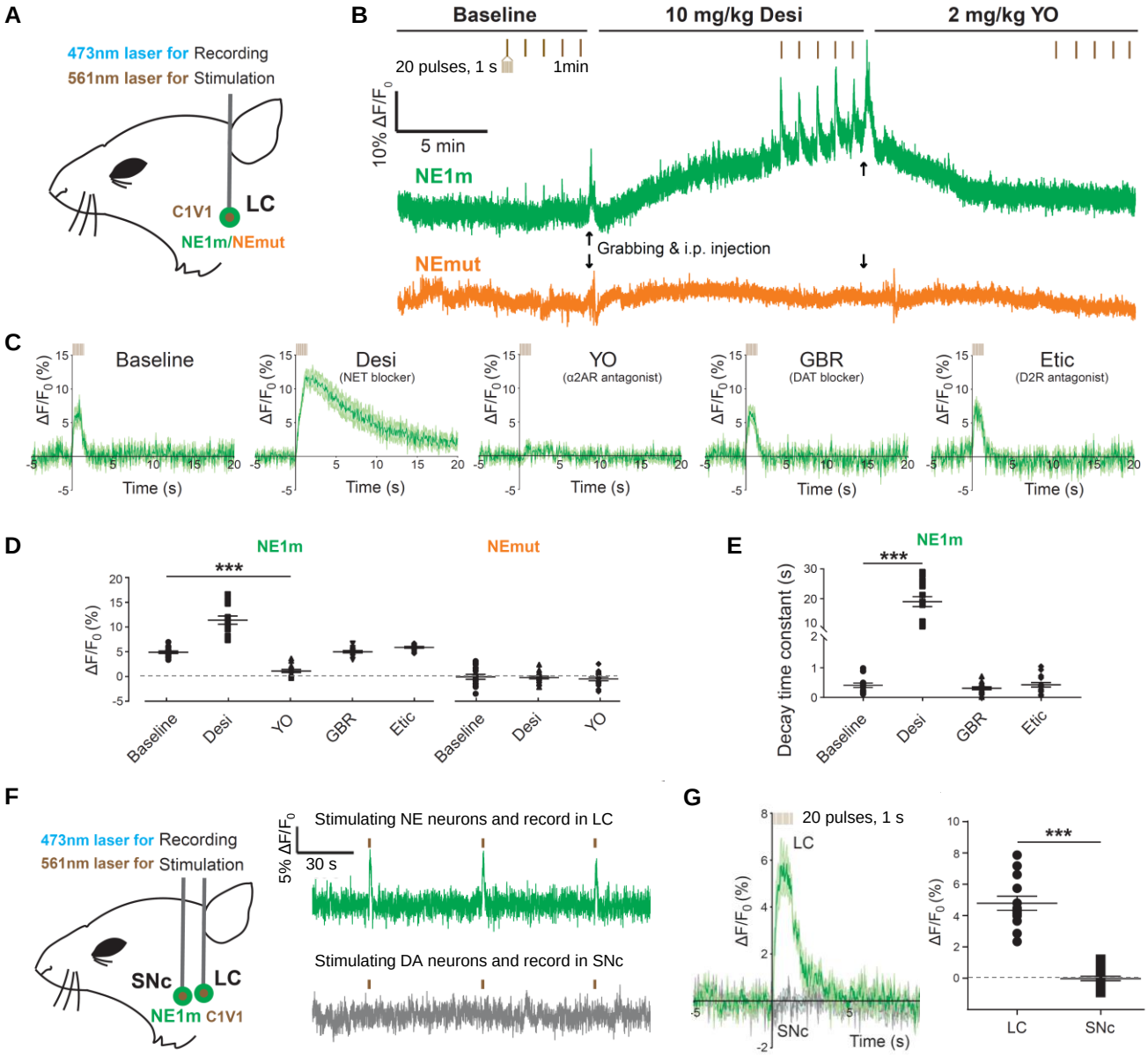
A
473nm laser for Recording
561nm laser for Stimulation
C1V1
LC
NE1m/NEmut
B
Baseline
10 mg/kg Desi
2 mg/kg YO
20 pulses, 1 s
1min
10% ΔF/F0
5 min
NE1m
Grabbing & i.p. injection
NEmut
C
Baseline
Desi
(NET blocker)
YO
(α2AR antagonist)
GBR
(DAT blocker)
Etic
(D2R antagonist)
ΔF/F0 (%)
Time (s)
D
NE1m
NEmut
***
ΔF/F0 (%)
Baseline
Desi
YO
GBR
Etic
E
NE1m
***
Decay time constant (s)
Baseline
Desi
GBR
Etic
F
473nm laser for Recording
561nm laser for Stimulation
SNc
LC
NE1m C1V1
Stimulating NE neurons and record in LC
5% ΔF/F0
30 s
Stimulating DA neurons and record in SNc
G
20 pulses, 1 s
LC
SNc
ΔF/F0 (%)
Time (s)
***
LC
SNc

Fig 7

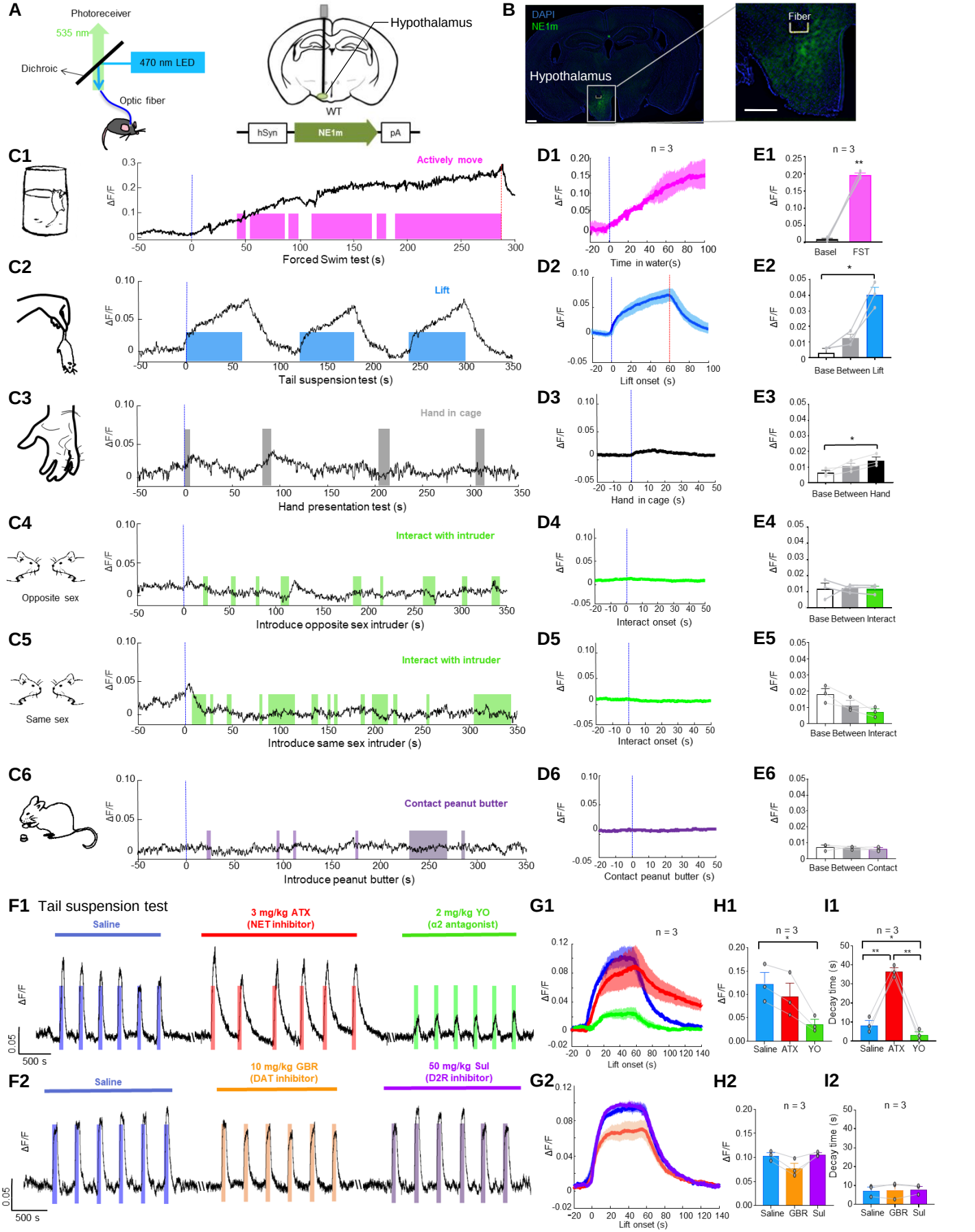
A
Photoreceiver
535 nm
Dichroic
470 nm LED
Optic fiber
Hypothalamus
WT
hSyn
NE1m
pA
B
DAPI
NE1m
Hypothalamus
Fiber
C1
Actively move
Forced Swim test (s)
C2
Lift
Tail suspension test (s)
C3
Hand in cage
Hand presentation test (s)
C4
Opposite sex
Interact with intruder
Introduce opposite sex intruder (s)
C5
Same sex
Interact with intruder
Introduce same sex intruder (s)
C6
Contact peanut butter
Introduce peanut butter (s)
D1
n = 3
Time in water(s)
D2
Lift onset (s)
D3
Hand in cage (s)
D4
Interact onset (s)
D5
Interact onset (s)
D6
Contact peanut butter (s)
E1
n = 3
Basel
FST
E2
Base Between Lift
E3
Base Between Hand
E4
Base Between Interact
E5
Base Between Interact
E6
Base Between Contact
F1 Tail suspension test
Saline
3 mg/kg ATX
(NET inhibitor)
2 mg/kg YO
(α2 antagonist)
500 s
F2
Saline
10 mg/kg GBR
(DAT inhibitor)
50 mg/kg Sul
(D2R inhibitor)
500 s
G1
n = 3
Lift onset (s)
G2
Lift onset (s)
H1
n = 3
Saline
ATX
YO
H2
n = 3
Saline
GBR
Sul
I1
n = 3
Decay time (s)
Saline
ATX
YO
I2
n = 3
Decay time (s)
Saline
GBR
Sul

Fig S1

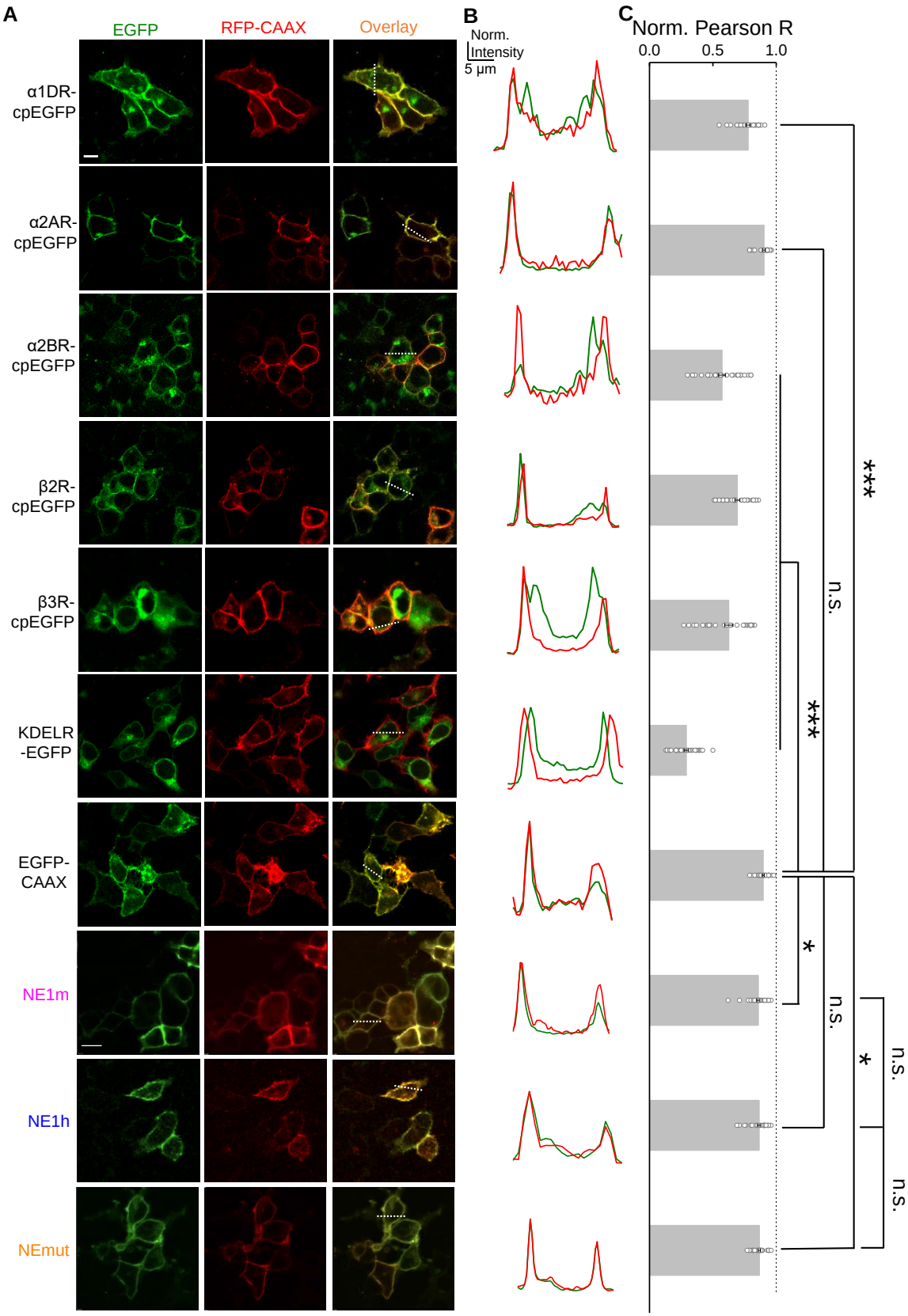
A
EGFP
RFP-CAAX
Overlay
α1DR-cpEGFP
α2AR-cpEGFP
α2BR-cpEGFP
β2R-cpEGFP
β3R-cpEGFP
KDELR-EGFP
EGFP-CAAX
NE1m
NE1h
NEmut
B
Norm. Intensity
5 µm
C
Norm. Pearson R
0.0
0.5
1.0
***
n.s.
***
*
n.s.
*
n.s.
n.s.

Fig S2

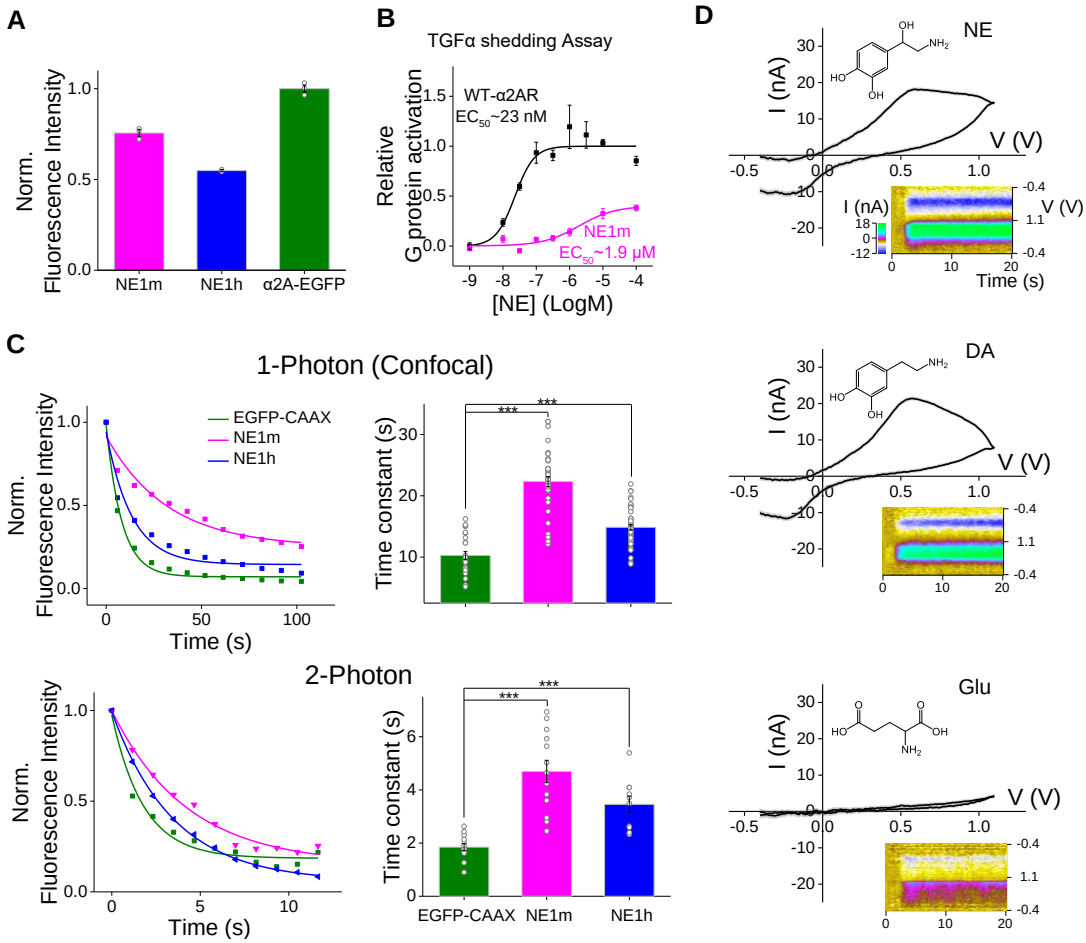
A
Norm. Fluorescence Intensity
NE1m
NE1h
α2A-EGFP
B
TGFα shedding Assay
Relative G protein activation
WT-α2AR
EC50~23 nM
NE1m
EC50~1.9 μM
[NE] (LogM)
C
1-Photon (Confocal)
EGFP-CAAX
NE1m
NE1h
Time (s)
Time constant (s)
2-Photon
D
NE
DA
Glu
I (nA)
V (V)
Time (s)

Fig S3

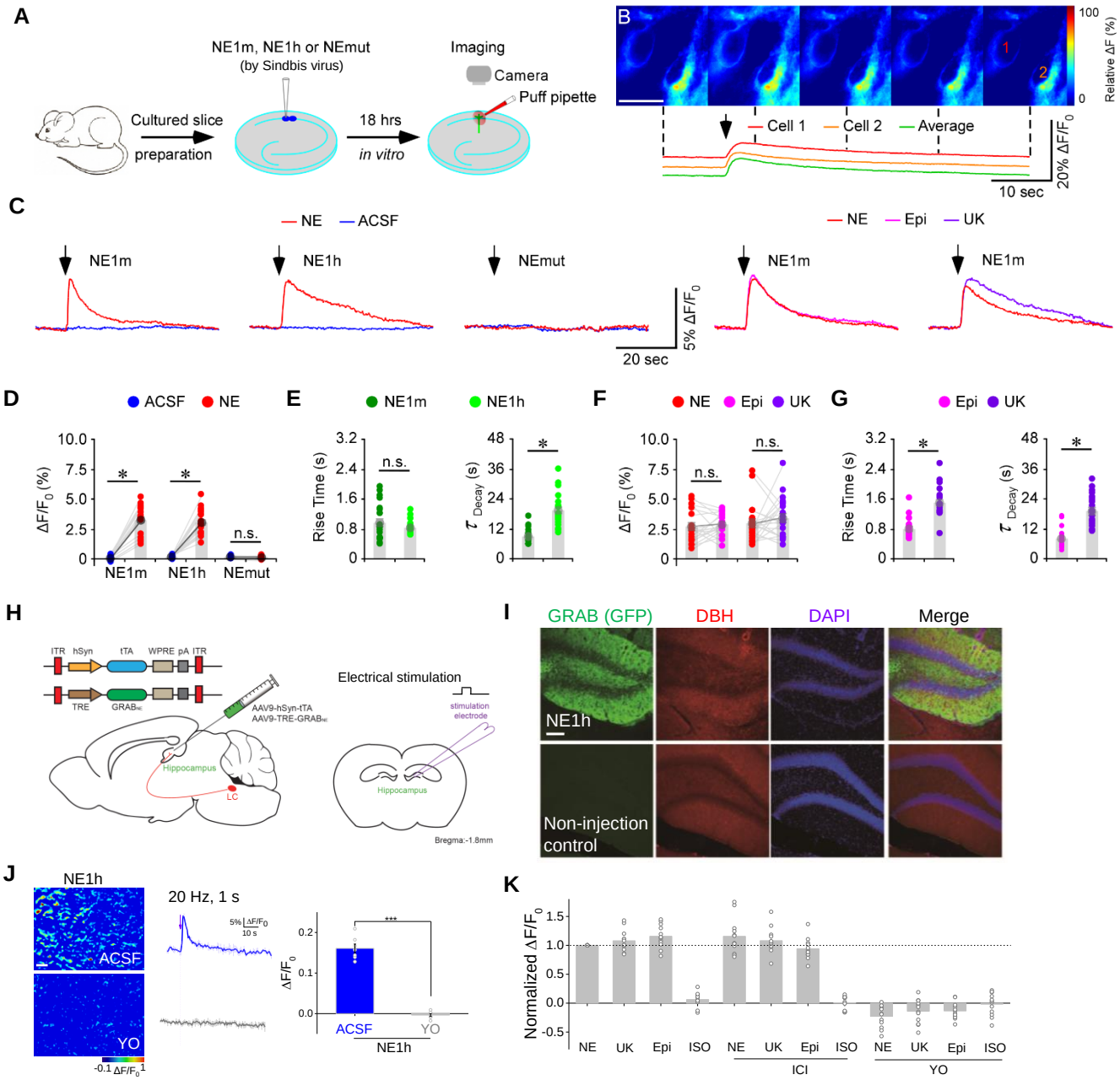
A
NE1m, NE1h or NEmut
(by Sindbis virus)
Imaging
Camera
Puff pipette
Cultured slice
preparation
18 hrs
in vitro
B
Relative ΔF (%)
Cell 1
Cell 2
Average
20% ΔF/F0
10 sec
C
NE
ACSF
NE1m
NE1h
NEmut
5% ΔF/F0
20 sec
NE
Epi
UK
D
ACSF
NE
ΔF/F0 (%)
NE1m
NE1h
NEmut
n.s.
E
NE1m
NE1h
Rise Time (s)
τ Decay (s)
F
NE
Epi
UK
G
Epi
UK
H
ITR
hSyn
tTA
WPRE
pA
TRE
GRABNE
AAV9-hSyn-tTA
AAV9-TRE-GRABNE
Hippocampus
LC
Electrical stimulation
stimulation electrode
Bregma:-1.8mm
I
GRAB (GFP)
DBH
DAPI
Merge
NE1h
Non-injection control
J
NE1h
ACSF
YO
-0.1 ΔF/F0 1
20 Hz, 1 s
5% ΔF/F0
10 s
ΔF/F0
ACSF
YO
NE1h
K
Normalized ΔF/F0
NE
UK
Epi
ISO
ICI
YO